The Meteoritical Society

Meteoritics & Planetary Science 49, Nr 1, 36–44 (2014)
doi: 10.1111/maps.12114

Dust coma of comet C/2009 P1 (Garradd) by imaging polarimetry

E. HADAMCIK[1*], A. K. SEN[2], A. C. LEVASSEUR-REGOURD[3], S. ROY CHOUDHURY[2], J. LASUE[4], R. GUPTA[5], and R. BOTET[6]

[1]UPMC, LATMOS, 11 Bld d'Alembert, 78280 Guyancourt, France
[2]Assam University, Silchar 788011, India
[3]UPMC, LATMOS, 4 Place Jussieu, 75005 Paris, France
[4]UPS, IRAP, BP 44346, 31028 Toulouse, France
[5]IUCAA, Postbag 4, Ganeshkhind, Pune, India
[6]Univ. Paris-Sud, LPS, Bat 510, 91405 Orsay, France
[*]Corresponding author. E-mail: edith.hadamcik@latmos.ipsl.fr

(Received 17 September 2012; revision accepted 08 March 2013)

Abstract–Comet C/2009 P1 (Garradd) was observed by imaging polarimetry for nearly 5 months from October 2011 to March 2012, over an intermediate phase angle range (28°–35°). Two months before perihelion and one month after, dust particles seem to be ejected all around the optocenter and jets extend to distances greater than 40,000 km. An increase of activity is noticed in intensity and polarization after perihelion. Two months before perihelion and one month after, the dust emission seems to be all around the optocenter. Two and three months after perihelion the jets are mainly toward the solar direction with an extension of more than 20,000 km projected on the sky. The values of the aperture polarization are comparable to those of other comets. On the polarization maps in October 2011 and January 2012 the higher polarization zones extend in large regions perpendicularly to the solar direction where jets are also observed. In February and March 2012, the polarization in the jets is larger in the solar direction than in the surrounding coma. By its activity visible on intensity images and polarization maps at large distances from the nucleus, comet Garradd probably belongs to the high-P_{max} class of comets.

INTRODUCTION

Comets have progressively been recognized as able to provide key information about the origin and early evolution of our solar system. Some of them are likely to have formed in the vicinity of giant planets before being stored much farther away in the Oort cloud and eventually returning as new active comets. Other ones are likely formed in the Kuiper Belt and transported in the inner solar system as periodic comets (e.g., Festou et al. 2004). Amongst new bright comets, comet C/2009 P1 Garradd (hereafter Garradd) was discovered in August 2009 by G. J. Garradd from Siding Springs Observatory in Australia at 8.7 AU from the Sun. This seemingly dynamically new comet presents an almost parabolic orbit. It reached its perihelion on 23 December 2011, at a solar distance (R) of about 1.5505 AU. Earth-based observations were favorable until early March 2012, where its distance to the Earth (Δ) went down to about 1.27 AU. Ground-based observations (Villanueva et al. 2012) and space-based observations from, e.g., Swift satellite and Deep Impact space probe (Bodevits et al. 2012) have indicated a large dust production rate, even far away from the Sun, suggesting that its activity might not only be triggered by water ice sublimation.

Cometary dust, ejected by sublimating ices gas drag into the low-density gaseous comae is efficiently studied by observations of solar scattered light and specifically from its partial linear polarization (e.g., Dollfus et al. 1988; Levasseur-Regourd et al. 1999; Hadamcik and Levasseur-Regourd 2003a). Such measurements are monitored as a function of (α), the phase angle between the directions of the Sun and of the observer as seen from the scattering dust and (λ), the wavelength of the observations, allowing comparisons of the dust properties between different regions of a given coma and between different comets. Comparisons to experimental and

Table 1. Instrumentation at OHP and IUCAA.

Observatory	Telescope diameter aperture	CCD resolution (binning)	Polarizer	Cometary continuum filters
OHP 5°43′E +43°56′	Cassegrain 0.8 m f/15	0.21 arcsec/pixel 4 × 4 pixels	Rotating 4 polaroids	ESA narrow band CB 443 nm, Δλ 4 nm CR 684 nm, Δλ 9 nm Broadband R_{OHP} 650 nm, Δλ 90 nm I_{OHP} 810 nm, Δλ 150 nm
IGO 73°40′E +19°5′	Cassegrain 2 m f/10	0.307 arcsec/pixel 1 × 1 pixel	Rotating half-wave plate + Wollaston prism	ESA narrow band CB 443 nm, Δλ 4 nm CR 684 nm, Δλ 9 nm Broadband R_{IGO} 630 nm, Δλ 120 nm I_{IGO} 900 nm, Δλ 80 nm

numerical simulations provide clues to the dust properties (Hadamcik et al. 2006, 2007a; Levasseur-Regourd et al. 2007; Lasue et al. 2009; Das and Sen 2011). We have observed comet Garradd in the context of a France-India research project. This collaboration, allowing polarimetric observations of the same small object from two different observing sites in the Northern hemisphere, Haute-Provence Observatory (OHP) in France and Girawali Observatory in India, has already provided results about, e.g., comet 67P/Churyumov-Gerasimenko, to better characterize its environment in preparation of the Rosetta mission that is to rendezvous with its nucleus in 2014 (Hadamcik et al. 2010). Comet Garradd observations, from October 2011 to March 2012, corresponded to increasing solar distances (R) from 1.33 to 1.93 AU, to decreasing Earth distances (Δ) from 2.10 to 1.33 AU, and to phase angles remaining between 28° and 35°, i.e., in a region where differences between cometary dust presenting a low polarization and cometary dust presenting a high polarization are already detectable.

We first describe the instrumental techniques, including the data reduction, and present the log of the observations. Then, we analyze the results about the brightness of the light scattered by dust and its decrease as a function of optocentric distance. The linear polarization is analyzed in terms of aperture polarization (allowing easy comparisons with other comets) and of polarization maps, before discussing the significance of these results for the properties of comet Garradd'dust.

OBSERVATIONS AND DATA REDUCTION

Two telescopes with a Cassegrain configuration were used: a 80 cm telescope at OHP in France and a 2 m telescope at IUCAA Girawali Observatory (IGO) in India. At OHP, four polaroids are mounted on a rotating wheel; the polarized components with their fast axis at 45° from one another are recorded successively. At IGO, a rotating half-wave plate and a Wollaston prism allow us to record two perpendicularly polarized components on the same CCD image (frame): in the next image the two components are polarized at 45° from the previous ones (for more details see Sen and Tandon 1994; Ramaprakash et al. 1998). Different continuum filters avoid or reduce contaminations by the gaseous emissions (Table 1). For more details on the instruments and data reduction, see, e.g., Hadamcik et al. (2010, 2013).

Four polarized components are obtained for each series of observations. The intensity (I), polarization (P), and polarization angle (θ) are calculated by the following expressions:

$$I = I_0 + I_{90} = I_{45} + I_{135} \tag{1}$$

$$P = 200\frac{\sqrt{(I_0 - I_{90})^2 + (I_{45} - I_{135})^2}}{I_0 + I_{90} + I_{45} + I_{135}} \tag{2}$$

$$\theta = 0.5 \arctan\frac{I_{45} - I_{135}}{I_0 - I_{90}} \tag{3}$$

$$\theta_r = \theta - \theta_0 - (\phi \pm 90) \tag{4}$$

The polarized intensities are measured in the instrumental reference system. $\theta_r = (\theta - \theta_0)$ is the position angle of the polarization plane in the equatorial reference system. The position angle of the scattering plane (ϕ) is known at each date. For symmetry reason it is defined between 0° and 180° and can be deduced from the value of the Sun-comet radius vector position angle (Sun-C PA in Table 2). The sign between the parentheses, in Equation 4, is chosen to ensure the

Table 2. Log of the observations.

Date	Δ (AU)	*R* (AU)	α (°)	Sun-C PA (°)	Filters	Resolution (km/pixel)
IGO, October 21–22, 2011	2.10–2.11	1.61	30.9–30.8	69–68	CB, CR	470
OHP, October 26, 2011	2.11	1.60	30.3	64	R_{OHP}	1290
OHP, January 23–25, 2012	1.68–1.64	1.60–1.61	34.8–35.2	317–315	CR, R_{OHP}	1030–1000
IGO, February 18–20, 2012	1.35–1.34	1.74	34.7–34.3	285–281	CR, R_{IGO}, I_{IGO}	300
OHP, March 17–19, 2012	1.37–1.33	1.96–1.93	28.5–28.3	172–165	CB, CR, R_{OHP}, I_{OHP}	840–810

Δ = distance to Earth; *R* = solar distance; α = phase angle; Sun-C PA = extended Sun-comet radius vector position angle (JPL Horizons ephemeris).

Table 3. Polarized and unpolarized standard stars.

	Star	*P* (%)	PA (°)	P_{obs} (%)	PA_{obs} (°)	θ_0
OHP October	HD236633 (R)	5.376 ± 0.028	93.04 ± 0.15	5.25 ± 0.10	92 ± 1	1
	HD21447 (B)	0.017 ± 0.03	28.63 ± 0.3	0.02 ± 0.02(R)	25 ± 4	4
	BD+59°389 (R)	6.43 ± 0.02	98.1 ± 0.02	6.20 ± 0.16	103 ± 2	−5
	HD251204 (R)	4.27 ± 0.028	147 ± 2	4.32 ± 0.10	138 ± 10	9
OHP January	HD21447 (B)	0.017 ± 0.03	28.63	0.02 ± 0.05	24 ± 5	5
	G191B2B	0.09 ± 0.06	147	0.02 ± 0.02	129 ± 10	18
	HD236633 (R)	5.376 ± 0.028	93.04 ± 0.21	5.41 ± 0.05	98 ± 8	−5
	HD94851 (B)	0.057 ± 0.018	NA	0.163 ± 0.0	67.5 ± 5	‘
	HD94851 (V)		NA	0.07 ± 0.05	89 ± 5	
IGO February	HD25443 (R)	4.734 ± 0.045	133.65 ± 0.28	4.854 ± 0.1	132.28 ± 1	1.5
	HD25443 (V)	5.127 ± 0.061	134.23 ± 0.34	5.1 ± 0.2	132.5 ± 5	2.3
	BD+59°389 (R)	6.43 ± 0.022	98.14 ± 0.10	6.4 ± 0.1	105 ± 8	−7
	BD+59°389 (V)	6.701 ± 0.015	98.09 ± 0.07	6.5 ± 0.1	91 ± 8	7
	HD94851 (B)	0.06 ± 0.02	NA	0.08 ± 0.10	91 ± 8	
OHP March	HD155197 (R)	4.274 ± 0.027	102.88 ± 0.18	4.1 ± 0.2	114 ± 5	1
	GD319 (B)	0.045 ± 0.047	140.79	0.07 ± 0.1	161 ± 10	−21
	GD319 (V)	0.089 ± 0.093	140.15	0.08 ± 0.1 (R)	135 ± 10 (R)	5
	HD155197	4.38 ± 0.03	103	4.05 ± 0.15	93 ± 10	10

Observations in red (R), blue (B), and (V) filters. *P* and PA from the literature (Turnshek et al. 1990; Schmidt et al. 1992), P_{obs} and PA_{obs} from observations, $\theta_0 = (PA - PA_{obs})$. NA = not available.

condition $0° < (\phi \pm 90°) < 180°$. θ_r is generally of about 90° for comets observed at phase angles larger than 25° (Levasseur-Regourd et al. 1996).

A center gravity algorithm is used to find the position of the optocenter of the comet on each polarized image. To avoid artifacts in the polarization maps, the polarized components are centered with a precision of better than 0.1 pixel before any calculation. The sky background is estimated in a region outside the coma and subtracted. Then, fluxes through apertures with diameters of 12 and 24 pixels centered on the optocenter are measured for each polarized components (I_0, I_{45}, I_{90}, and I_{135}), and their stability in each aperture is controlled as well as the total intensity *I* (Equation 1) for the whole series. If a difference greater than 2% is detected between the fluxes measured on the successive images, the image is rejected.

The log of the observations is presented in Table 2, together with the filters used for each run. During the October 2011 observations the sky was partially cloudy at both sites, for OHP observations on a run of 4 nights, only 4 h were acceptable. In January and February 2012, the comet was only observable during 2 or 3 h at the end of the nights. During each night, polarized and unpolarized stars were observed to estimate the residual instrumental polarization and to determine the origin of the instrumental reference system θ_0 (Table 3).

RESULTS

Intensity variations and coma morphologies are presented from October 2011 to March 2012. Then, variations of the linear polarization are discussed.

Intensity Images

The polarized components are added to build the intensity images for each filter (Equation 1). The azimuthally averaged radial log-log profile is studied first

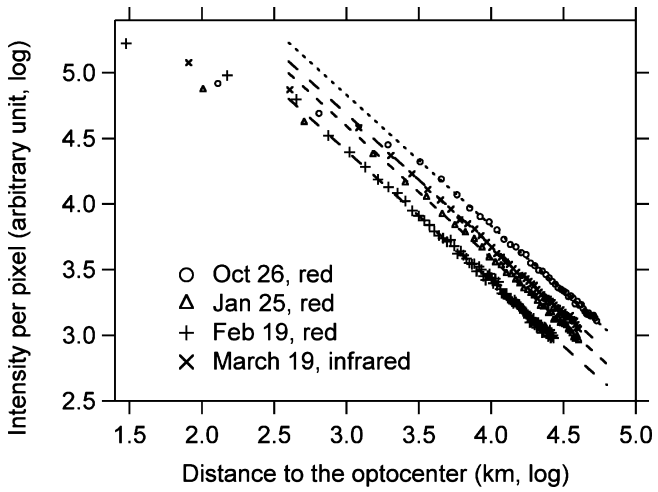

Fig. 1. Azimuthally averaged radial intensity profiles for the four periods of observations and fits with a (−1) slope.

(Fig. 1). For all the runs, the slope of decrease is nominal (-1 ± 0.05) from the optocenter as expected from an isotropic coma (out of the blurred central region by seeing). This nominal (−1) slope at large optocentric distances indicates that the sky background has been correctly subtracted for each series of observations.

The overall shape of the coma is circular in projection on the sky with a limited sunward-tailward asymmetry. Figure 2 presents isophotes levels in the left column. Intensity images analyzed by a rotational gradient method (Larson and Sekanina 1984)—to emphasize the azimuthal intensity gradients generally corresponding to jet structures—are presented in the right column. For all observing periods, the main feature is more developed in the projected solar direction. In projection, it extends over more than 40,000 km. During October, the jets present several fan structures. One fan structure with PA ≈ [240°–310°] is close to the solar direction (PA = 244°) while there is another one in the antisolar direction with PA ≈ [50°–130°]. In January, the jets seem to be curved anticlockwise all around the optocenter with a slightly larger extension in the solar direction (PA = 135°). Close to the optocenter three different ejecting directions are noticed with PA ≈ 110°, PA ≈ 5°, and PA ≈ 325° (not easily seen on the gray-scale image). During February, structures are well observed in the solar direction with fan-shaped fine jets between PA ≈ [85°–120°] (solar PA = 105°) and on the two sides shorter jets at PA ≈ 55° and PA ≈ 115°. Projected on the sky, the main jets extend over more than 22,000 km long. The structures are similar during the three nights of observations through the cometary red and infrared filters. During March observations, a V-shaped

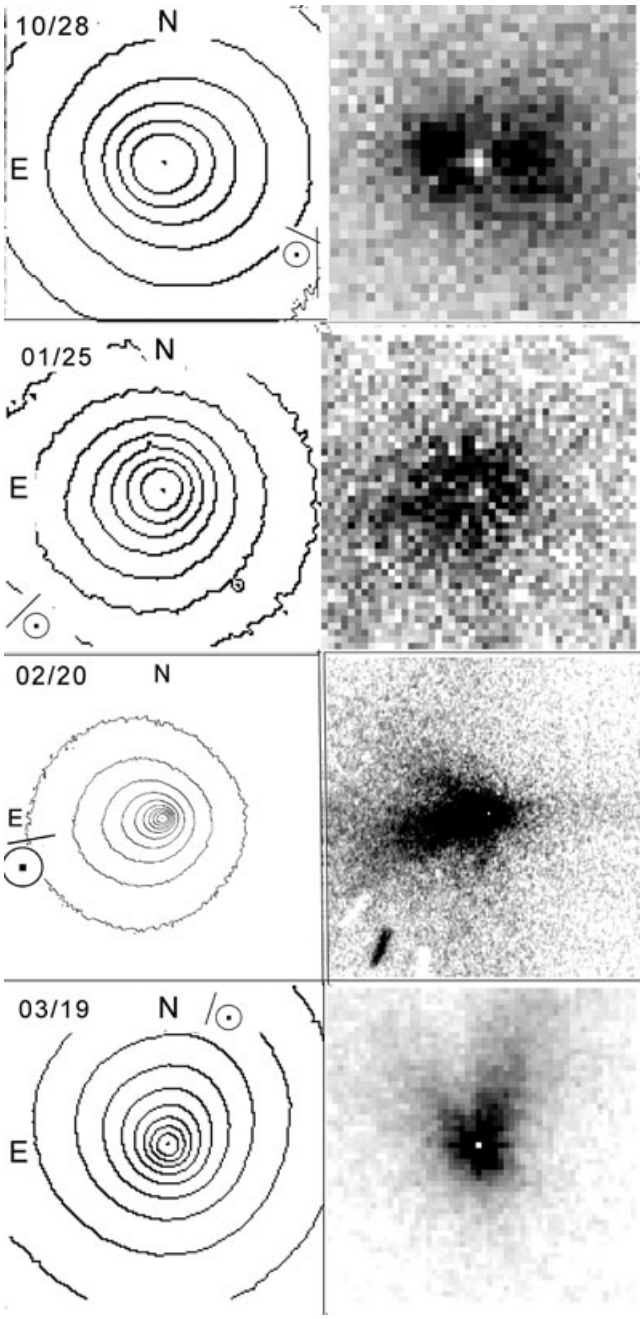

Fig. 2. Intensity images for October, January, February, and March. Left column: isophotes with the solar direction indicated by a line with ⊙. Right column: images of intensity treated by a rotational gradient method (in negative). Fields 45,000 × 45,000 km. North is up and East is left.

structure is observed. Its longer branch is oriented in the solar direction, with an extension of more than 40,000 km at a PA ≈ 340°. The shortest branch has an extension of more than 12,000 km on the sky with a PA ≈ 35°. Close to the optocenter the ejection seems to be mainly in the South direction (about antisolar). For

the three nights of observation in March, similar structures are observed with all the filters.

Figure 3a compares the radial decrease profiles in intensity between the solar and antisolar directions as a function of the optocentric distance for the four periods. The profiles present similar overall shapes with a higher intensity in the solar direction up to more than 25,000 km from the optocenter. The slope values can be found in Table 4. The slope increases progressively with the optocentric distance in the solar direction, indicating that dust is moving from this region. A slope smaller than −1 indicates that dust is pushed tailward by the solar radiation replenishing the antisolar regions. Figure 3b and Table 4 compare the decrease profiles in intensity between the two perpendicular directions to the solar direction. The differences between these profiles are very small, as generally observed.

The changing solar distance can explain the change in the structures as compared to the solar directions between the four runs, with more activity after perihelion (January and February). It also depends on different geometric configurations related to the orientation and projection of the jets as seen from the Earth.

Linear Polarization

Aperture polarization is obtained for each period and filter (Equation 2). The values are compared with values on the synthetic phase curves for other comets. On the polarization maps, regions with a higher polarization than the surrounding coma are detected, suggesting differences in the physical properties of the dust.

Aperture Polarization

The fluxes are measured through different apertures on the polarized component images (sum of all the selected images for each orientation of the polarization). The polarization is calculated using Equation 2. It also provides the determination of the integrated polarization whenever the cometary tracking is imperfect. The results are presented in Table 5 and in Fig. 4A. The position angle of the polarization plane in the equatorial reference system (related to the solar PA) θ_r is on average about 90° (calculated by Equations 3 and 4 in an aperture of about 50 pixels diameter) for all the observations, without any variation close to the

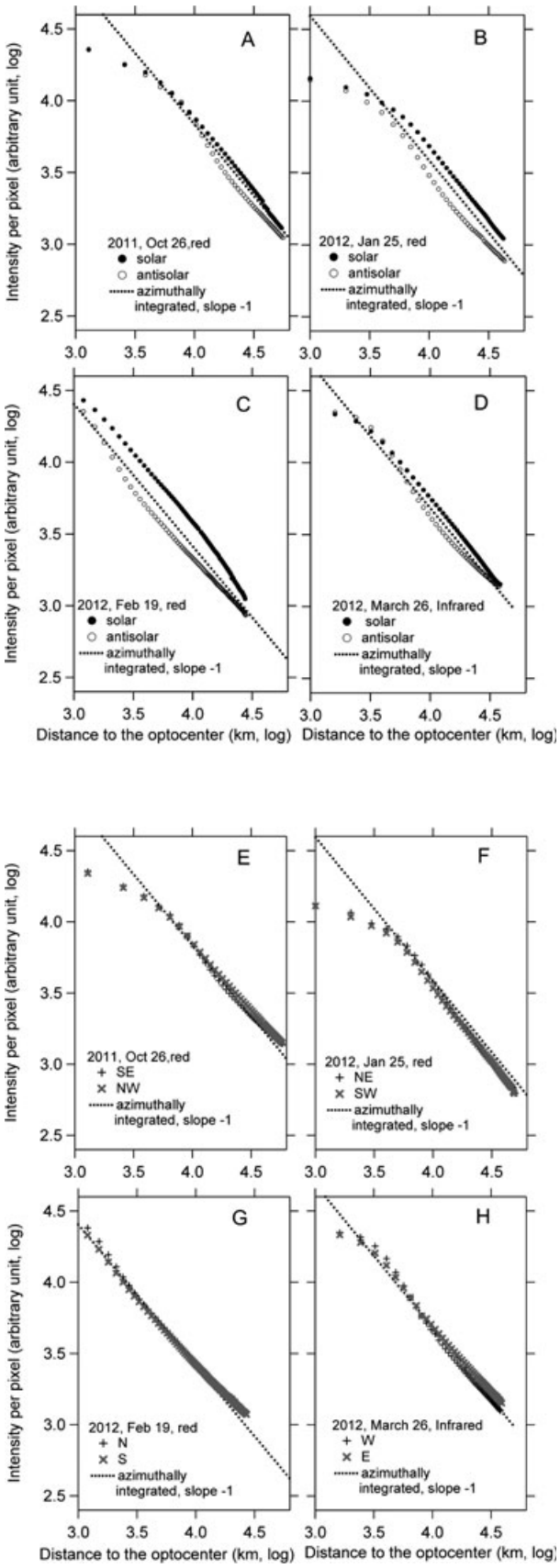

Fig. 3. a) Profiles as a function of optocenter distance for comparison of intensity decrease between the solar and antisolar directions for each period of observations. b) Profiles as a function of optocenter distance for comparison of intensity decrease between the perpendicular directions to the solar directions for each period of observations.

Table 4. Slopes in log–log scale in the solar (S), antisolar (anti-S) directions, and in the perpendicular (⊥) directions for the four runs of observations.

Date		Distance to optocenter (10^3 km)							
		1	3	7	10	20	30	40	50
October	S	/// <		-0.87	><	-1.02	><	-1.17	>
	antiS	/// <		-0.87	><	-1.13	><	-0.89	>
	⊥ SE	////////<	-0.76	><	-0.97	> <	-0.79		>
	⊥ NW	////////<		-0.86	><		-0.82		>
January	S	//// <-0.62>			-1.01	><	-1.05		>//////
	antiS	//// <-1.03><	-1.2	><		-0.84			>//////
	⊥ NE	//////<-0.67><	-1.2	><		-1.1	><	-0.99	>///////
	⊥ SW	//////<				-0.92			>///////
February	S	<-0.88><-0.94><	-1.10	><		-1.33	>//////////////////////////////////////		
	antiS	<-1.36><-0.96><			-0.87		>//////////////////////////////////////		
	⊥ N	<-1.16><-1.06><	-0.94	><	-0.88	><	-0.76	>//////////////////////////////////////	
	⊥ S	<-0.96><	-1.10	><	-0.86	><	-0.79	>//////////////////////////////////////	
March	S	// < -0.95 ><		-1.00	><		-1.10		>/////
	antiS	// < -1.40 ><		-0.97	><		-0.74		>/////
	⊥ W	// <-0.29><		-1.19	><		-0.90		>/////
	⊥ E	// <-0.42><		-1.03	><		-0.87		>/////

For February at IGO, the limitation of the measurements to 30,000 km allows to avoid any overlapped region between the two polarized components in the same image.

optocenter. The wavelength dependence is presented in Fig. 4B. As expected for such phase angles no significant differences are observed between the polarization values outside the error bars.

Polarization Maps

Polarization maps for the four periods are presented in Fig. 5. The different regions have polarization values different only by about 1%, which is at the limit of the error bars. The structures are observed over successive nights and for different combinations of the series of polarized components. In the regions where a higher polarization is observed, a slight increase in intensity is also observed on the profiles (October: Fig. 3b(E) NW; January: Fig. 3b(F) NE, optocentric distance $d < 15000$ km; February: Fig. 3a(C) E solar direction; March: Fig. 3a(D) solar direction and Fig. 3b(H) W for $d < 8000$ km).

1. In October (Fig. 5A), the central region presents a polarization of ≈2.6% and increases slightly in the North–West direction shaping an extending arc structure (Sun is about South-West) with a polarization of ≈3%. The difference is small but this structure is observed in different combinations of the series of images and seems to be real.
2. In January (Fig. 5B), the higher polarization region extends North–East from PA ≈ 20° to PA ≈ 120°, close to the solar direction. The maximum polarization value is about 6% while in the South-West opposite direction it is about 4%.
3. In February (Fig. 5C), the central region presents a polarization value between 3% and 5% at the center. It extends on average up to 7000 km distance. The polarization in the surrounding region has an apparent width around the central region of about 12,000 km with a value of approximately 3% and decreases farther away. Whenever jets appear on the treated intensity image (East direction), they are also present on the polarization map with approximately 4% polarization (the surrounding polarization being 3%). Their extension is greater than 20,000 km.
4. In March (Fig. 5D), the central region—with an average polarization of about 4%—is elongated (East–West) with an extension of 9000 km and a width of 4000 km. Farther away a symmetric "butterfly" shape is observable on both sides extending over 14,000 km with an average polarization value of 3%. In the outer coma, the polarization value falls down to 1%. The butterfly wings extend further toward the Sun.

Table 5. Polarization values (in %) for different apertures and wavelengths. Error bars correspond to a confidence level of 95% (2σ).

Date 2011–2012	Day (UT)	Aperture diameter filter	5000 km	10,000 km	20,000 km	30,000 km	40,000 km	θ_r (°)
IGO October	21	CB	2.6 ± 0.4	2.5 ± 0.5	2.8 ± 0.7	2.3 ± 0.8	NA	88 ± 10
(α = 30.9°–30.8°)	22	CR	2.9 ± 0.3	2.8 ± 0.2	2.8 ± 0.6	2.6 ± 0.6	NA	
		CB	2.8 ± 0.5	2.7 ± 0.4	2.3 ± 0.6	2.1 ± 0.8	NA	
		CR	2.7 ± 0.5	2.6 ± 0.4	2.5 ± 0.5	2.5 ± 0.6	NA	
OHP October	26	R_{OHP}	2.6 ± 0.5	2.8 ± 0.4	2.8 ± 0.4	2.7 ± 0.4	2.6 ± 0.4	94 ± 10
(α = 30.3°)								
OHP January	23	R_{OHP}	NA	3.3 ± 0.5	4.1 ± 0.4	4.5 ± 0.5	4.2 ± 0.6	89 ± 10
(α = 34.8°–35.2°)	24	CR	NA	4.7 ± 0.2	4.7 ± 0.3	4.2 ± 0.6	4.1 ± 0.6	75 ± 10
	25	CR	5.7 ± 0.4	4.8 ± 0.3	4.7 ± 0.3	4.7 ± 0.3	3.8 ± **0.5**	85 ± 8
IGO February	18	R_{IGO}	3.6 ± 0.3	3.7 ± 0.3	3.7 ± 0.3	3.7 ± 0.4	3.6 ± 0.5	88 ± 5
(α = 34.7°–34.3°)		CR	3.7 ± 0.2	3.6 ± 0.3	3.6 ± 0.3	3.5 ± 0.5	3.3 ± 0.5	99 ± 10
	19	I_{IGO}	3.9 ± 0.2	3.8 ± 0.2	3.6 ± 0.3	3.5 ± 0.4	3.2 ± 0.5	97 ± 10
	20	I_{IGO}	3.8 ± 0.3	3.9 ± 0.2	3.8 ± 0.2	3.7 ± 0.2	3.6 ± 0.5	88 ± 10
		CR	3.9 ± 0.3	3.7 ± 0.4	3.7 ± 0.4	3.6 ± 0.5	3.5 ± 0.5	
		R_{IGO}	3.9 ± 0.2	3.9 ± 0.3	3.8 ± 0.3	3.8 ± 0.4	3.5 ± 0.5	
		CR	3.9 ± **0.3**	3.7 ± 0.4	3.6 ± 0.5	3.7 ± 0.5	3.2 ± 0.6	
OHP March	18	R_{OHP}	2.2 ± 0.3	2.1 ± 0.2	2.2 ± 0.2	2.1 ± 0.2	2.0 ± 0.3	89 ± 5
(α = 28.5°–28.3°)	19	CR	2.1 ± 0.3	2.3 ± 0.3	2.2 ± 0.2	2.2 ± 0.3	2.1 ± 0.3	90 ± 3
		CR	2.3 ± 0.3	2.25 ± **0.3**	2.3 ± 0.2	2.2 ± 0.2	2.2 ± 0.3	
	20	1_{OHP}	5.0 ± 0.5	3.2 ± 0.2	2.9 ± 0.2	2.8 ± 0.3	2.5 ± 0.3	90 ± 4
		CB	NA	1.9 ± 0.4	2.0 ± 0.4	1.9 ± 0.5	NA	
		CB	NA	2.1 ± 0.4	2.2 ± 0.4	2.0 ± 0.5	NA	
		CR	2.1 ± 0.3	2.3 ± 0.3	2.3 ± 0.3	2.2 ± 0.3	2.1 ± 0.3	
		R_{OHP}	2.3 ± 0.3	2.3 ± 0.2	2.2 ± 0.2	2.1 ± 0.3	2.1 ± 0.3	
		I_{OHP}	4.1 ± 0.4	2.6 ± 0.2	2.4 ± 0.3	2.0 ± 0.3	2.0 ± 0.3	

Amongst the four periods of observations, the smaller solar distance and the larger phase angle are in January. This can be the reason why the polarization is slightly higher during this time. The decrease in Earth-to-comet distance allows a higher resolution in the two last periods but the activity seems to decrease with the decrease in the solar distance from January to March.

DISCUSSION AND CONCLUSION

Linear polarization measurements of the light scattered by dust on comet Garradd have also been performed by Kiselev et al. (2012), between August 2011 and February 2012 at phase angles of about 13°, 15°, 22°, 30°, 31°, 32°, and 37°. The polarization values perfectly agree with our results and complement them.

The polarization values remain constant when the aperture is sufficiently large before decreasing at the dust coma limit (Table 5). This behavior is usually observed in comets. To point out similarities and differences in the dust ejected by comet Garradd and by other comets, the polarization values are compared with observations of other comets. From the available data in the literature, synthetic polarization phase curves were built in different wavelength domains in the visible (Levasseur-Regourd et al. 1996). Two classes were defined: (1) with a low maximum in polarization of about 10–15%, (2) with a higher polarization and a maximum of about 25–30%. Trigonometric fits define synthetic phase curves for the two classes and the wavelength domains (blue-green, red, near-infrared). The classification is generally possible once measurements are available at phase angles larger than 35°. The results for comet Garradd are similar to those obtained for other comets (Fig. 4A), perhaps closer to the high-P_{max} comets class (but the difference between high and low-P_{max} comets is small at phase angles smaller than 35°). Bodevits et al. (2012) suggest similarities between comet Garradd and comet Hale-Bopp. The polarization values of comet Hale-Bopp are much higher than those obtained for any other comets (Levasseur-Regourd 1999), including presently studied comet Garradd indicating at least different physical properties for their dust.

New and periodic comets have both been observed by imaging polarimetry at low or intermediate phase angles. High-P_{max} comets present generally well structured jets with a higher polarization than the

surrounding coma and extending at relatively large distances from their nucleus as compared with the coma size. The presence of submicron-sized grains, in highly porous large aggregates, has been suggested in the jets and arcs of comet Hale-Bopp (Hanner et al. 1997; Hayward et al. 2000; Hadamcik and Levasseur-Regourd 2003b). More generally, the particles in the jets of high-P_{max} comets seem to be made of similar grains and structures but the number of the jets is relatively smaller. In the coma of low-P_{max} comets, structures may be absent on the polarization maps, e.g., in comet C/1989 X1 Austin (Eaton et al. 1992) or high polarization regions with small extension around the optocenter may be found. In that case, the ejected dust probably consists of large dark particles, moving slowly and eventually breaking down. This seemed to be the case for comet 9P/Tempel 1 before the Deep Impact event and comet 67P/Churyumov-Gerasimenko before perihelion (Hadamcik et al. 2007b, 2010). The jets in comet Garradd are preferentially oriented in the solar direction. On the polarization maps, jets are mainly observable in January, February, and in March. Their extension is more than 20,000 km. Their properties are consistent with a population of submicron to micron-sized grains in aggregates. In January and February the higher polarization and extension of the jets may be the result of an increase in activity after perihelion. On March maps, the higher polarization region is relatively restricted but the butterfly-shaped structure may be the result of particles breaking up after leaving the central high polarization region. Such behavior has been observed, e.g., around the main fragment of comet C/1999 S4 (LINEAR) during its complete disintegration (Hadamcik and Levasseur-Regourd 2003c).

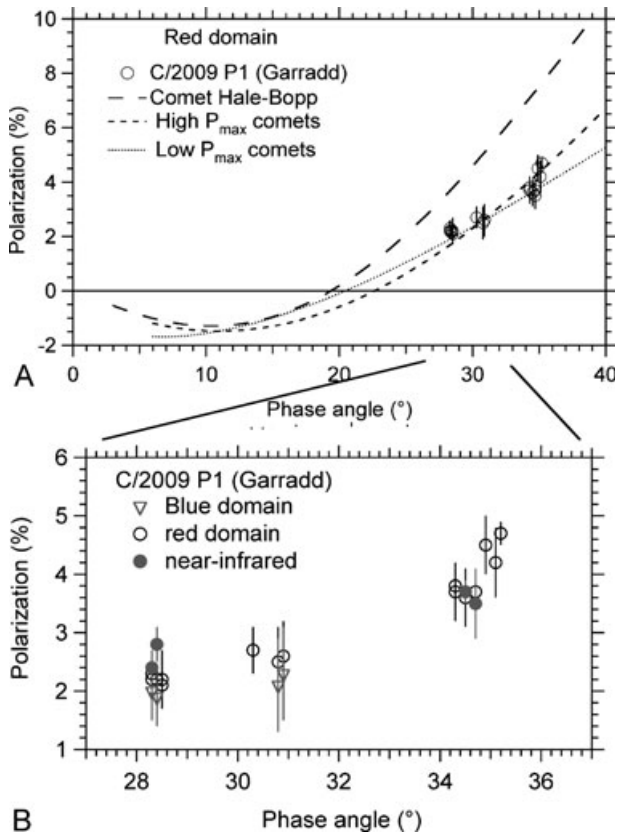

Fig. 4. Polarization curves. Up: in the red wavelength domain with comparison to other comets. Down: Comparison between data obtained at different wavelengths.

In conclusion comet Garradd was observed during five observational runs from October 2011 to March 2012. The phase angle varies between 28° and 35°. The linear polarization of the scattered light by the dust particles is similar to those of other comets. Jet activity is observed on each period. After perihelion, in January, February, and March, higher polarization jets are apparent in the solar direction. This activity seems to confirm a classification among the high-P_{max} class of comets with ejection of small submicron to micron-sized grains possibly in aggregates.

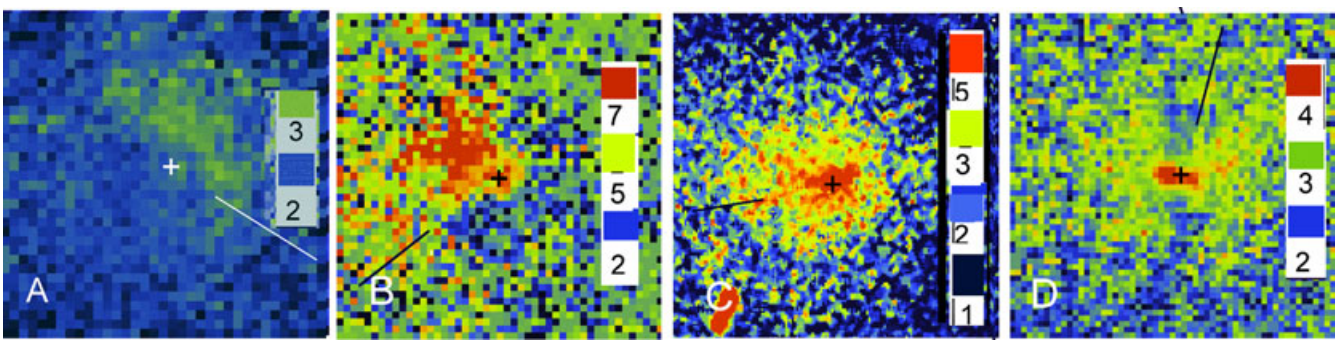

Fig. 5. Polarization maps: A) 2011 October (R_{OHP} filter), B) 2012 January (RC filter), C) February (R_{IGO} filter), D) March (I_{OHP} filter) observations. To improve the display a Gaussian filter was applied. Optocenter +, straight line: solar direction. Color or gray scales in percent. Fields 45,000 × 45,000 km. North is up and East is left. Some images have been treated by a median filter.

Acknowledgments—We thank Daniel Bardin for his help in the observations at OHP. We gratefully acknowledge ESA for the narrow-band filters at OHP. OHP and IUCAA are acknowledged for allocation of observation time. The authors are part of a CEFIPRA project team (India-France CEFIPRA Research Project No. 4507-1). A. C. L. R. acknowledges support from the French Space Agency (CNES).

Editorial Handling—Dr. Donald Brownlee

REFERENCES

Bodevits D., Farnham T. L., A'Hearn M. F., and Landsman W. B. 2012a. Swift observations of the long term activity of comet C/2009 P1 (Garradd). Proceedings of the Asteroids, Comets, Meteors conference 2012, Nigata, Japan. LPI Contribution 1667. Houston, Texas: Lunar and Planetary Institute. p. id.6084.

Bodevits D., Farnham T. L., and A'Hearn M. F. 2012b. Comet C/2009 P1 (Garradd). Electronic Telegram 3090, IAU.

Das H. S. and Sen A. K. 2011. Model for cometary grains to explain optical polarization. *Journal of Quantitative Spectroscopy & Radiative Transfer* 112:1833–1837.

Dollfus A., Bastien P., Le Borgne J. F., Levasseur-Regourd A. C., and Mukai T. 1988. Optical polarimetry of P/Halley: Synthesis of the measurements in the continuum. *Astronomy & Astrophysics* 206:348–356.

Eaton N., Scarrott S. M., and Gledhill T. M. 1992. Polarization studies of comet Austin. *Monthy Notices of the Royal Astronomical Society* 250:654–656.

Festou M. C., Keller H. U., and Weaver H. A., eds. 2004. *Comets II*. Tucson: University of Arizona Press. 780 p.

Hadamcik E. and Levasseur-Regourd A. C. 2003a. Imaging polarimetry of cometary dust: Different comets and phase angles. *Journal of Quantitative Spectroscopy & Radiative Transfer* 79–80:661–679.

Hadamcik E. and Levasseur-Regourd A. C. 2003b. Dust evolution of comet C/1995 O1 (Hale-Bopp) by imaging polarimetric observations. *Astronomy & Astrophysics* 403:757–768.

Hadamcik E. and Levasseur-Regourd A. C. 2003c. Dust coma of comet C/1999 S4 (LINEAR): Imaging polarimetry during nucleus disruption. *Icarus* 166:188–194.

Hadamcik E., Renard J.-B., Levasseur-Regourd A. C., and Lasue J. 2006. Light scattering by fluffy particles with the PROGRA^2 experiment: Mixtures of materials. *Journal of Quantitative Spectroscopy & Radiative Transfer* 100:143–156.

Hadamcik E., Renard J.-B., Rietmeijer F. J. M., Levasseur-Regourd A. C., Hill H. G. M., Karner J. M., and Nuth J. A. 2007a. Light scattering by fluffy Mg-Fe-SiO and C mixtures as cometary analog (PROGRA^2 experiment). *Icarus* 190:660–671.

Hadamcik E., Levasseur-Regourd A. C., Leroi V., and Bardin D. 2007b. Imaging polarimetry of the dust coma of comets Tempel 1 before and after Deep Impact at Haute-Provence Observatory. *Icarus* 190:459–468.

Hadamcik E., Sen A. K., Levasseur-Regourd A. C., Gupta R., and Lasue J. 2010. Polarimetric observations of comet 67P/Churyumov-Gerasimenko during its 2008–2009 apparition. *Astronomy & Astrophysics* 517:A86.

Hadamcik E., Sen A. K., Levasseur-Regourd A. C., Gupta R., Lasue J., and Botet R. 2013. Dust in comet 103P/Hartley 2 coma during EPOXI mission. *Icarus* 222:774–785.

Hanner M. S., Gehrz R. D., Harker D. E., Hayward T. L., Lynch D. K., Mason C. C., Russell R. W., Williams D. M., Wooden D., and Woodward C. E. 1997 (published in 1999). Thermal emission from the dust coma of comet Hale-Bopp and the composition of the silicate grains. *Earth, Moon, and Planets* 79:247–264.

Hayward T. L., Hanner M. S., and Sekanina Z. 2000. Thermal infrared imaging and spectroscopy of comet Hale-Bopp (C/1995 01). *The Astrophysical Journal* 538:428–455.

Kiselev N. N., Rosenbush V. K., Afanasiev V. L., Blinov D. A., Kolesnikov S. V., and Zaitsev S. V. 2012. Comparative polarimetry of comets 103P/Hartley 2, 9P/Tempel 1 and C/2009 P1 (Garradd). Proceedings of the Asteroids, Comets, Meteors Conference 2012, Nigata, Japan. LPI Contribution 1667. Houston, Texas: Lunar and Planetary Institute. p. id.6102.

Larson S. M. and Sekanina Z. 1984. Coma morphologies and dust-emission pattern of periodic comet Halley. I—High resolution images taken at Mount Wilson in 1910. *The Astronomical Journal* 89:571–578.

Lasue J., Levasseur-Regourd A. C., Hadamcik E., and Alcouffe G. 2009. Cometary dust properties retrieved from polarization observations: Application to C/1995 O1 Hale-Bopp and 1P/Halley. *Icarus* 199:129–144.

Levasseur-Regourd A. C. 1999. Polarization of light scattered by cometary dust particles: Observations and tentative interpretations. *Space Science Reviews* 90:163–168.

Levasseur-Regourd A. C., Hadamcik E., and Renard J. B. 1996. Evidence for two classes of comets from their polarimetric properties at large phase angle. *Astronomy & Astrophysics* 313:327–333.

Levasseur-Regourd A. C., McBride N., Hadamcik E., and Fulle M. 1999. Similarities between in situ measurements of local dust scattering and dust flux impact data within the coma of 1P/Halley. *Astronomy & Astrophysics* 348:636–641.

Levasseur-Regourd A. C., Mukai T., Lasue J., and Okada Y. 2007. Physical properties of cometary and interplanetary dust. *Planetary and Space Science* 55:1010–1020.

Ramaprakash A. N., Gupta R., Sen A. K., and Tandon S. N. 1998. An imaging polarimeter (IMPOL) for multiwavelength observations. *Astronomy & Astrophysics, Supplement Series* 128:369–375.

Schmidt G. D., Elston R., and Lupie O. 1992. The Hubble space telescope northern-hemisphere grid of stellar polarimetric standards. *The Astrophysical Journal* 104:1564–1567.

Sen A. K. and Tandon S. N. 1994. A two channel optical imaging polarimeter. In *Instrumentation in astronomy VIII, proceedings SPIE*, edited by Crawford D. L. and Craine E. R. vol. 2198. International Symposium on Astronomical Telescope and Instrumentation for Twenty First Century, Kona, Hawaii. pp. 264–273.

Turnshek D. A., Bohlin R. C., Williamson R. L., II, Lupie O., Koornneef J., and Morgan D. H. 1990. An atlas of Hubble Space telescope photometric, spectrometric, and polarimetric calibration objects. *The Astrophysical Journal* 99:1243–1261.

Villanueva G. L., Mumma M. J., DiSanti M. A., Bonev B. P., Paganini L., and Blake G. A. 2012. A multiinstrument study of comet C/2009 P1 (Garradd) at 2.1 AU (pre-perihelion) from the Sun. *Icarus* 220:291–295.

Journal of Quantitative Spectroscopy & Radiative Transfer 146 (2014) 444–451

Contents lists available at ScienceDirect

Journal of Quantitative Spectroscopy & Radiative Transfer

journal homepage: www.elsevier.com/locate/jqsrt

A study of comet 78P/Gehrels by imaging polarimetry

S. Roy Choudhury [a,*], E. Hadamcik [b], A.K. Sen [a]

[a] Department of Physics, Assam University, Silchar 788011, India
[b] UPMC University Paris 6, LATMOS, IPSL-CNRS, 11 Bld d'Alembert, 78280 Guyancourt, France

ARTICLE INFO

Article history:
Received 15 October 2013
Received in revised form
8 February 2014
Accepted 9 February 2014
Available online 17 February 2014

Keywords:
Comet 78P/Gehrels
Scattering
Polarization
Cometary dust
Technique: imaging polarimetry

ABSTRACT

Comet 78P/Gehrels was observed polarimetrically from the 2 m telescope at IUCAA Girawali Observatory (IGO) in India and from the 0.8 m telescope at Haute-Provence Observatory (OHP) in France. The observations were carried out in three schedules – first in October 2011 (IGO), then in January 2012 (OHP) and lastly in February 2012 (IGO), when its phase angle was between 15.2° and 28.3°. In our knowledge, these are the first polarimetric measurements of the dust properties of Gehrels. Both broadband and narrow band cometary filters (to avoid gaseous contaminations) were used. Intensity images treated by a rotational gradient method, along with isophotes confirmed the presence of structures in the comet during the observation periods. In the polarization map, no significant difference in polarization values is noticed between the structures along the anti-solar direction and the surrounding coma, which suggests similar dust properties. After perihelion, in January, some jet activity was observed along the solar direction with higher positive polarization than the surrounding coma. The ejected particles seem to be relatively large and present with a low number density. The coma polarization measured in different apertures has been used to compare that obtained for other comets at similar phase angles. As expected, 78P/Gehrels is different from comet Hale–Bopp, but the comparison is not easy at phase angles lower than 35°.

1. Introduction

Comet 78P/Gehrels, also known as Gehrels 2, is a periodic Jupiter Family comet. It was discovered at magnitude 15–16, during a minor planet survey in 1973, by Tom Gehrels of Lunar and Planetary Laboratory, Arizona, USA, while examining plates exposed with 122-cm Schmidt Telescope of Palomar Observatory. Numerous immediate observations allowed us to calculate the precise elliptical orbit indicating a perihelion date of November 30, 1973 and an orbital period of 7.93 years. The comet's aphelion of 5.4 au is in the zone of control of the giant planet Jupiter and the orbit of the comet is frequently perturbed (http://sites.google.com/site/robsastropics/comets-78p-gehels [13], http://cometography.com/pcomets/078p.html [14]).

The concerned comet is a poorly studied one. A'Hearn et al. [2] from one observation at a heliocentric distance of 2.36 au after perihelion had classified the comet as carbon-chain depleted. Fink and Hicks [4] observed the comet on October 9, 1989, at a heliocentric distance of 2.35 au and obtained a spectrum which seems to be missing of notable gaseous emissions. Lowry and Weisman [19] observed it on May 24, 2001, at a heliocentric distance of 5.5 au before perihelion; the comet was active and its nucleus radius was estimated to be 1.41 ± 0.12 km if an albedo of 0.04 was assumed. Snodgrass et al. [25] observed the comet on March 2, 2006, at a heliocentric distance of 3.84 au after perihelion; the comet was active. Mazotta Epifani and Palumbo [20] with a multicolor UBVRI broadband photometry observed the comet on October 27, 2004, at a heliocentric distance of 2 au, some days after perihelion

* Corresponding author. Mobile: +91 8011206221.
E-mail address: saumya.viv@gmail.com (S. Roy Choudhury).

http://dx.doi.org/10.1016/j.jqsrt.2014.02.010
0022-4073

and close to the Earth. The comet was bright and showed a well-developed coma with a tail-like structure and an important solar, antisolar asymmetry. A surface brightness slope was deduced and found to be -1.54 ± 0.02. Some axisymmetric lobes were detected on treated images (red and infrared filters) but difficult to further interpret.

In complement to photometric and spectroscopic observations, linear polarization studies give some indications for the optical and physical properties inside the coma. Previous observations through similar polarimetric imaging methods (e.g. [23,22,5,6]) have allowed the different regions in the coma to be confirmed. Noted features include high polarization in the jets, a region with a deeper negative branch at small phase angles or lower polarization in the positive branch in a restricted region close to the nucleus but not observed in all comets (polarimetric halo). The different physical properties are indicated by the values of the polarization together with the brightness variations, but some coma variations are not yet completely interpreted. In a joint campaign some Indian and French astronomers (authors of the present paper) under CEFIPRA (Indo French Centre for the Promotion of Advanced Research) funded project jointly observed some comets such as 67P/Chruryumov-Gerasimenko, which are targets of the Rosetta spacecraft in 2014–2015. The long-time polarization evolution reveals emission of large particles before perihelion and fluffy faster particles just after perihelion, these different dust emissions seem correlated to the nucleus rotation and illumination [9]. Comet 103P/Hartley 2 observations include the period of fly-bye by the deep impact spacecraft during the EPOXI mission. The high polarization regions correspond to the jets as emphasized by the nucleus rotation [10]. Comet C/2009 P1 (Garradd) coma structures and polarization were found to be changing with the solar distance. A further increase of activity, a higher polarization near perihelion and fine extended jets after perihelion were observed [11].

Under the same joint campaign, comet 78P/Gehrels was observed in polarimetric mode by Indian and French astronomers from two observatories viz. IGO and OHP simultaneously, located in India and France respectively. These observations along with analysis are being reported in the present work. It was observed for 2 nights in October 2011 from IGO; about 3 months before the perihelion. In January 2012; just 12 days after the perihelion it was observed for 1 night from OHP. Lastly, 1 month after that, the comet was again observed for 2 nights in February 2012 from IGO. During the observing periods the comet's geocentric distance increased from 1.21 to 2.28 au, the visual magnitude lied between 11.5 and 12.6, and its solar phase angle varied between 15.2° and 28.3°. The data have been reported from http://ssd.jpl.nasa.gov/horizons.cgi [12].

These polarimetric observations, at our knowledge, are the first of its kind for this relatively faint comet. Another motivation for the observations is the small phase angle and the possibility to deduce the inversion angle and perhaps the chance to observe once more the deep negative polarization region around the nucleus (polarimetric halo) detected in some comets [6]. In this paper we present the analysis of broadband R filter and narrowband CR filter images of 78P/Gehrels. The observations made with CCD as detector permits recording of changes of dust activity within coma with time. In the next section we describe the instrumentation and provide details on the observation log and the data reduction. Then, we present brightness and polarization results, discussions followed by conclusions. In results, we show our analysis on the brightness of the light scattered by dust and its decrease as a function of optocentric distance. The linear polarization is analyzed in terms of aperture polarization and polarization maps and compared in the discussion to other comets' polarization values at similar phase angles.

2. Observations and data reductions

The observations were made with two telescopes in Cassegrain configuration: one in India and another in France. Starting with the instruments and its working formulae, the observation log and data reduction procedure are discussed below.

2.1. Instruments

IGO: The IUCAA (Inter University Center for Astronomy and Astrophysics) Girawali Observatory, 'IGO' is situated near Pune, India. It is located at 19°5′N latitude, 73°40′E longitude, 1000 m altitude.

The Cassegrain telescope has a diameter of 2 m and focal ratio $f/10$. An instrument called IFOSC (IUCAA Faint Object Spectrograph and Camera) containing a rotating half-wave plate (HWP) and a Wollaston prism is used to measure polarization. The field of view for polarization imaging has a 4 arcmin and the resolution of CCD camera used is 0.307 arcsec diameter by pixel.

The rotating HWP with its fast axis normal to the optical axis of the system is associated to a Wollaston prism. When the HWP rotates successively 22.5°, 45° and 67.5° from an initial position denoted 0, the position angles of the polarized components respectively rotate 45°, 90°, and 135° from the initial position. At each position of the HWP, two orthogonally polarized beams are recorded at the same time on the CCD frame. The separation between the ordinary and extraordinary components is 0.9 arcmin. Two successive positions of the HWP are needed to retrieve the degree of polarization and the position angle of the polarization vector (for more details on the instrument, see [24,21]). The telescope tracking-mode was cometary by differential tracking.

The intensity (I), polarization (P), and polarization angle (θ) are calculated by the expressions

$$I = I_o(\beta)+I_e(\beta) \tag{1}$$

$$R(\beta) = \frac{\frac{I_e(\beta)}{I_o(\beta)}-1}{\frac{I_e(\beta)}{I_o(\beta)}+1} \tag{2}$$

$$P = 100\sqrt{R(\beta)^2+R(\beta+22.5)^2} \tag{3}$$

$$\theta = 0.5\arctan\left[\frac{R(\beta+22.5)}{R(\beta)}\right] \tag{4}$$

where β corresponds to different HWP positions with respect to the celestial NS-axis. $\beta=0^\circ$, 22.5°, 45°, 67.5°. $R(\beta)=q$ when $\beta=0^\circ$, 45° and $R(\beta)=u$ when $\beta=22.5^\circ$, 67.5°; where q, u are normalized Stoke's parameters.

OHP: The Observatory of Haute-Provence, 'OHP' is situated near Marseille, France. Observatory reference-511 in http://ssd.jpl.nasa.gov/horizons.cgi [12].

The Cassegrain telescope has a diameter of 0.8 m and focal ratio *f*/15. The field of view for polarization imaging is 7 arcmin on the side. The CCD camera has 2048×2048 pixels, back-illuminated, of 13.5 μm each. The resolution by pixel is thus 0.21 arcsec. The CCD is cooled down to -50 °C by a 5-stage Peltier system. A 4×4 pixels binning is used. The telescope tracking-mode was stellar to avoid any noticeable movement of the center during the 120 s exposers. Because the comet is faint, the signal-to-noise ratio is increased through building each polarized image by adding the 10 individual images for each position of the fast axis.

Four polaroid filters are mounted on a rotating wheel, with their fast axis oriented at 45° from one another, the first one corresponding to the so-called direction Zero '0'. For each orientation, a polarized intensity image is recorded (so-called $I_0, I_{45}, I_{90}, I_{135}$). For more details on the instruments, see Hadamcik et al. [9], Hadamcik et al. [10].

The intensity (I), the measured polarization (P), and polarization angle (θ) and are calculated by the expressions

$$I = I_0 + I_{90} = I_{45} + I_{135} \tag{5}$$

$$P = 200\frac{\sqrt{(I_0 - I_{90})^2 + (I_{45} - I_{135})^2}}{I_0 + I_{90} + I_{45} + I_{135}} \tag{6}$$

$$\theta = 0.5\arctan\left[\frac{I_{45} - I_{135}}{I_0 - I_{90}}\right] \tag{7}$$

Correlation between the notation of the polarized components of two observatories. For OHP, the fast axis position 0°, 90° (noted I_0, I_{90}) corresponds to position $\beta=0$ of HWP. Similarly (I_{45}, I_{135}), (I_{90}, I_0), (I_{135}, I_{45}) of OHP corresponds to position $\beta=22.5^\circ$, 45°, 67.5° of HWP respectively.

The position angle of the polarization plane relative to the plane perpendicular to the scattering plane

$$\theta_r = \theta - \theta_0 - (\phi \pm 90) \tag{8}$$

$(\theta-\theta_0)$ being the position angle of the polarization plane measured in the equatorial reference system. θ is the position angle of the polarization plane in the instrumental reference system and θ_0 is the position angle of the polarization axis of one polarized filter (measured for each period by observation of standard stars). The position angle of the scattering plane (ϕ) is known at each date. For symmetry reason it is defined between 0° and 180° and can be deduced from the value of the Sun–comet radius vector position angle (PA in Table 2). The sign between the parentheses, in Eq. (8), is chosen to ensure the condition $0^\circ < (\phi \pm 90^\circ) < 180^\circ$. θ_r is generally of about 0° for comets observed at phase angles larger than inversion angle (about 22°) and 90° for that observed below inversion angle. The polarization $P_r = P\cos(2\theta_r)$, with $P_r = P$ for $\theta_r=0^\circ$ and $P_r = -P$ for $\theta_r=90^\circ$.

Table 1 describes the central wavelength and band pass of various filters used during observations. One narrow-band ESA comet red (CR_{IGO}) filter and a broadband Bessel red filter (R_{IGO}) were used at IGO. At OHP, a Thuan–Gunn red filter (R_{OHP}) was used. The CR_{IGO} filter defined by ESA is used to avoid gaseous contaminations in the red continuum. In the R_{IGO} filter, the remaining contaminations may exist mainly by C_2, NH_2 and [OI]. They are reduced in the R_{OHP} filter for which NH_2 is the main eventual contaminant. The comet at large distance (3.3 au) did not show emission lines, but at smaller heliocentric distance, the comet may be more active with some more gaseous emissions. Nevertheless, the comet is found to be depleted in C_2 by A'Hearn et al. [2], at similar heliocentric distance than our observations and in that case the main contamination may be by NH_2.

Table 1
Central wavelength and band passes of the filters.

Filter	Central wavelength, λ (nm)	Band pass, $\Delta\lambda$ (nm)	Possible contaminations
ESA comet red, CR_{IGO}	684	9	None
Bessel red, R_{IGO}	630	120	C_2, NH_2, [OI]
Thuan–Gunn red, R_{OHP}	655	90	(C_2), NH_2, [OI]

2.2. Log of observations

During each night, polarized and unpolarized stars were observed along with the concerned comet at the same periods that the observations of comet C/2009 P1 (Garradd); the standard stars' results can be found in Hadamcik et al. [11]. A brief overview on the observations log together with the filters used for each run is presented in Table 2. Here α=phase angle, PA=Sun–comet radius vector position angle, m_V=visual magnitude, Δ=distance of the comet from the earth, and R=distance of the comet from the sun.

Table 2
Log of observations of comet 78P/Gehrels.

Observatory and observation period	α (deg)	PA (deg)	m_V	Δ (au)	R (au)	Resolution (km/pixel)	Filters
IGO; 21–22 October 2011	15.2	72	11.49	1.21	2.12	270	CR_{IGO}, R_{IGO}
OHP; 24 January, 2012	28.3	68	12.26	2.00	2.01	1200	R_{OHP}
IGO; 19–20 February, 2012	25.5	71	12.61	2.28	2.03	500	R_{IGO}

2.3. Data reduction

At first, all the individual images are bias subtracted and flat field corrected. Next, using a gravity center algorithm, the position of the optocenter of the comet on each image is determined. To avoid artifacts, the polarized components are centered with a precision of 0.1 pixels. Though for February observations, due to faintness of images, it is not always possible to have such a high precision on the centering.

After that, fluxes through apertures with diameters of 5, 10, and 15 pixels centered on the optocenter are measured for each polarized component ($I_0, I_{45}, I_{90}, I_{135}$) and their stability in each aperture is controlled as well as the total intensity I using Eqs. (1) and (5) for the whole series. If a difference greater than 3% is detected between the fluxes measured on the successive images, the image is rejected. But, for February a difference slightly greater than that is allowed. Then the sky background is estimated from a region outside the coma and free of faint stars. The aperture polarization described in Section 3.2 is calculated by using Eq. (3) and any background subtraction in the case of IGO is not necessary. But for OHP, the background is subtracted from each polarized component to measure polarization using Eq. (6). For intensity images described in Section 3.1, background is subtracted from each polarized component for both the observatories. The standard stars are used to estimate the residual instrumental polarization and to determine the origin of the instrumental reference system θ_0.

3. Results

For the three observational periods, azimuthally integrated radial intensity decrease, variations of intensity in different directions in the coma, coma morphologies and aperture linear polarization results and polarization maps have been presented in this section.

3.1. Intensity images

Intensity images are obtained by adding two mutually orthogonal polarized components, keeping in notice that their centers are precisely matched. For IGO, the components are the ordinary and extraordinary portions of an image for each HWP position and that for OHP are either (I_0, I_{90}) or (I_{45}, I_{135}). The successive intensity images thus obtained have to be similar and so, all the intensity images obtained for a particular set are added to build the final intensity images.

3.1.1. Intensity radial profile

First of all, a decrease in intensity along the radius is studied from the intensity images. To do that, the total intensity value is calculated in increasing apertures for each radial distance from the optocenter. From the aperture intensity values, the intensity in 1 pixel thickness annulus is computed out, and then divided by the number of pixels in that annulus. The log of the intensity values as a function of log of radial distance (in km) from optocenter is called azimuthally averaged radial intensity log–log profile (profiles in Fig. 1). For an isotropic coma, the slope of decrease would be nominal (-1). At large distances from the optocenter, the (-1) slope indicates that all the ejected dust moves in average progressively away from the nucleus and the sky background has been subtracted properly.

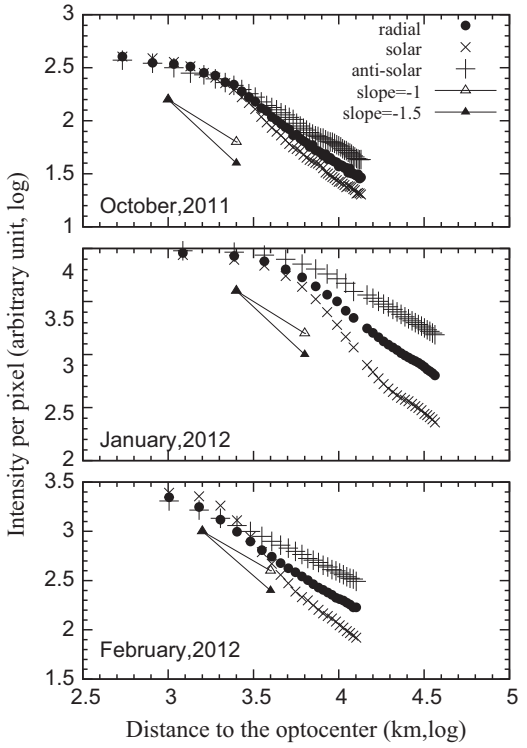

Fig. 1. Azimuthally integrated radial profiles of intensity, along with the profiles of decrease in intensity along solar and anti-solar directions, as a function of optocentric distance in log–log scale for the three periods of observations and fits with -1 slope.

Fig. 1 compares the azimuthally integrated radial profiles with a decrease in intensity along the solar and anti-solar directions as a function of the optocentric distance in log–log scale for October, January and February. The azimuthally integrated profiles are first considered. For October 2011; the slope is found to be about -1 for radial distance larger than 5400 km from optocenter. It is below -0.7 within the radial distance 2400 km. Between 2400 and 5400 km, there is a more pronounced decrease with slope -1.38. For January, the slope around -1 (-1.03) is detected in a region from 11,000 km to 19,500 km. Further away, a faint star tracks in the field of view. Between 2440 and 4880 km the slope is found to be -1.38 and that between 5000 km and 11,000 km is -1.33. For February 2012, the slope is around -1 for optocentric distance larger than 8000 km. From 2500 to 5000 km, the slope is about -1.23 and between 5000 and 8000 km it is about -1.08.

For October observation, it is found that the slope along anti-solar is slightly smaller than -1 (~ -0.95) after 2400 km. Prior to that, the slope is -0.55 from 1600 km to 2400 km. For January and February observations also, the slope along anti-solar is slightly smaller than -1 (~ -0.90) at large distances from optocenter. During

January, the slope is −0.30 between 2440 km and 7320 km and −0.92 between 7320 km and 45,000 km. In February, it is −0.71 from 1500 km and 3000 km, −0.79 between 3000 km and 7000 km, −0.85 between 7000 km and 12,500 km. But along the solar direction, values of slope are quite higher than −1. During October, the slope increases stiffly progressively from −0.87 between 1350 km and 2400 km to −1.56 between 2400 km and 5400 km. During January and February also, the slope along solar profile is found to be greater than −1. For February, it is −0.63 from 2440 km to 6100 km, −1.99 from 6100 km to 18,300 km and −1.13 from 20,000 km to 36,600 km. For February, the slope is −0.74 between 1500 km to 2000 km, −1.55 from 2000 to 2500 km, −2.12 from 2500 km to 5000 km, −1.8 from 5000 km to 10,000 km.

3.1.2. Coma morphologies

In this section isophotes and treated intensity images by a rotational gradient method [16] are presented (Fig. 2).

Isophotes: The isophotes reveal the asymmetry of the coma in projection on the sky. The shape of the coma during October 2011; i.e. 3 months before perihelion was slightly deflected from circularity with an elongation towards the antisolar direction and a structure at about a position angle of 165°. At that period of observation, the comet was at a phase angle of 15.2° and the Sun–comet PA was 72°. After perihelion, during January and February 2012, the coma is found to be clearly asymmetric, with tailward extension; the Sun–comet PA being 68° and 71° respectively.

Treated intensity images: The rotational gradient method is used to emphasize azimuthal intensity gradients, which help to identify jet structures. In the present study, only rotational shifts have been applied. In October 2011 at phase angle 15.2°, 3 months before perihelion, as on the isophotes a small structure can be noticed at about a position angle of 165°, on the treated intensity image; it is also detected on the isophotes. In the rotational gradient images of January and February, 2012, a distinct structure is observed tailward. The Sun–comet PA during those two periods was 68° and 71° respectively. The structure extensions are about 25,000 km in projection on the sky. In January, a sunward relatively short, 7000 km, dust ejection is also observed; it is fainter in February. The appearance and disappearance of structures during the three runs can be explained by varying phase angle, solar position angle and perihelion distance during each run. At low phase angle (15.2°), the dragged materials are about along the line of sight of observer and projected on the same direction on the sky. The direction of ejection of the materials can change with the solar direction PA and with the rotational axis of the nucleus.

3.2. Linear polarization

The variation in polarization values with an increase in aperture size is studied first. Next, polarization values are plotted as a function of phase angle. Finally, the polarization maps are obtained to detect variation in polarization in different regions of coma.

3.2.1. Aperture polarization

To calculate aperture polarization, at first, integrated flux through apertures on each orthonormally polarized component image corresponding to different positions of HWP (for IGO) and polaroid (for OHP) are measured. Then, aperture polarization is obtained from these integrated fluxes using Eq. (3) for IGO, Eq. (6) for OHP.

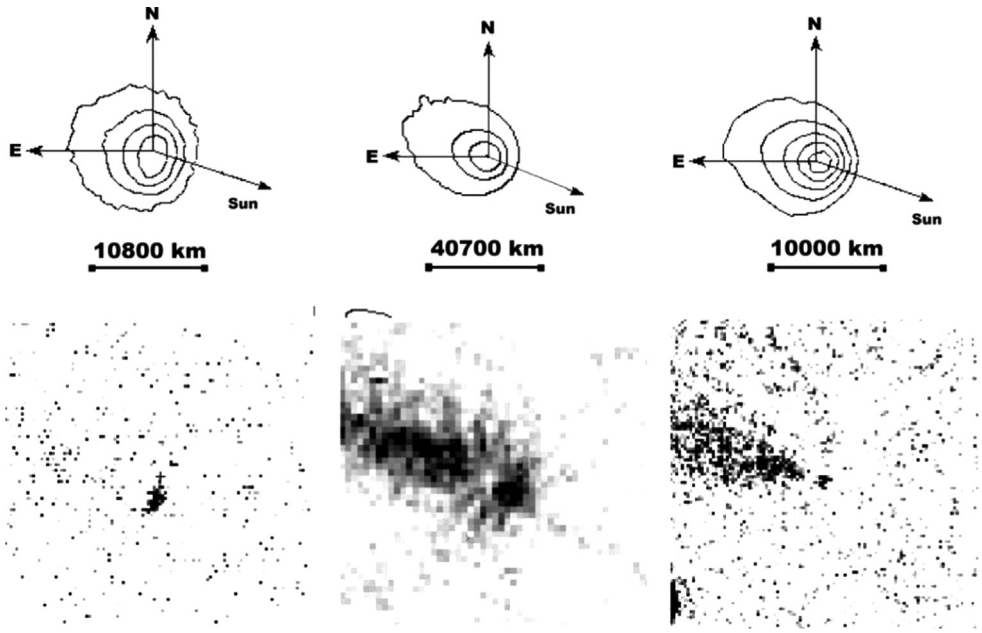

Fig. 2. Morphologies in intensity, from left: October 2011; January 2012; February 2012 respectively at phase angles of 15.2°, 28.3°, 25.5°. Upper line: isophotes in log scale. Lower line: intensity images treated by a rotational gradient method.

The polarization through increasing aperture sizes is presented in Table 3 for the different filters and periods. For the whole set of observations a decrease of polarization values is observed with increasing aperture. Nevertheless, this decreasing trend in polarization values with increasing aperture size is within the error bars. For October, the systematic lower value of polarization through the red broad R_{IGO} filter than through the cometary narrow red CR_{IGO} filter may be attributed to contaminations by emission lines of the gaseous species but the difference is smaller than the error bars. The good correlation with the synthetic phase curve in the positive branch indicates that the contamination is small (Fig. 4).

The origin of instrumental reference system θ_0 for January and February is on average 18° and 2° respectively [11]. The angle θ_r between position angle of polarized plane and scattering plane is about 0° for January and February. The θ_0 for October is 125° and θ_r about 90°. There is no significant variation of θ, and thus θ_r through the coma. As expected, the polarization value P_r is negative for $\alpha = 15.2°$ and positive for $\alpha > 25°$. As the observations were performed within a small range of phase angle, between 15.2° and 28.3°, it is very difficult to draw a reliable phase curve. But the polarization values will be compared in Section 4, to those found for other comets and synthetic phase curves.

3.2.2. Polarization maps

Polarization maps (Fig. 3) are obtained by processing the four polarization components of a particular set as a whole, using Eqs. (3) and (6). The variation of θ_r through coma being insignificant, the polarization values do not change sign on the polarization map. For October, the difference in polarization noticed on the polarization map along the observed structure at 165° is within the limit of error. But the polarization is slightly more negative around the optocenter, though the expected deep polarization is not observed. For January, on the polarization map, an eventual slightly greater polarization in the sunward direction can be observed. For February, on the polarization maps there is no difference of polarization along the tailward structure that appeared on the treated intensity image and the surrounding coma.

4. Discussion

4.1. Intensity variations in the coma

In the azimuthally integrated radial intensity profiles, it is noted that the slope of intensity decrease is nominal (slope −1) at large optocentric distances for all the periods of observation. The log–log profiles of intensity decrease between solar and anti-solar directions for all periods of observation indicate a higher intensity along the solar direction. The slope is found to increase progressively with the optocentric distance in the solar direction and that along the antisolar direction is found to decrease for all periods. A slope greater than −1 along the solar direction indicates that dust is moving away from the region. And along the anti-solar region, a slope smaller than −1 indicates that dust is pushed tailwards replenishing the region. So, it is understandable that the dusts are driven towards the anti-solar direction by solar radiation.

Table 3
Polarization values P_r (in %) for different apertures and wavelengths.

Observatory and period	α(deg)	Filter	2160 (km)	4320 (km)	7560 (km)	10,800 (km)	15,120 (km)	20,520 (km)	θ_r(deg)
IGO									
21 October 2011	15.2	CR_{IGO}	-1.2 ± 0.3	-1.1 ± 0.2	-0.7 ± 0.1	-0.8 ± 0.1	-0.8 ± 0.1	-0.8 ± 0.1	93 ± 10
		R_{IGO}	-0.9 ± 0.2	-0.8 ± 0.2	-0.8 ± 0.1	-0.6 ± 0.1	-0.6 ± 0.1	-0.5 ± 0.1	
22 October 2011		CR_{IGO}	-0.8 ± 0.4	-0.8 ± 0.3	-0.8 ± 0.2	-0.9 ± 0.1	-0.8 ± 0.1	-0.8 ± 0.1	89 ± 10
				4880 (km)	7320 (km)	9760 (km)	19,520 (km)	24,400 (km)	
OHP									
24 January 2012	28.3	R_{OHP}		2.4 ± 0.2	2.2 ± 0.2	2.0 ± 0.2	1.6 ± 0.2	1.5 ± 0.3	-3 ± 10
			2000 (km)	4000 (km)	7000 (km)	10,000 (km)	15,000 (km)	20,000 (km)	
IGO									
19 February 2012	25.5	R_{IGO}	1.3 ± 0.3	1.1 ± 0.2	1.1 ± 0.2	1.0 ± 0.2	0.7 ± 0.1	0.6 ± 0.1	4 ± 10
20 February 2012			1.1 ± 0.3	1.1 ± 0.2	0.9 ± 0.2	0.7 ± 0.1	0.6 ± 0.1	0.6 ± 0.1	3 ± 10

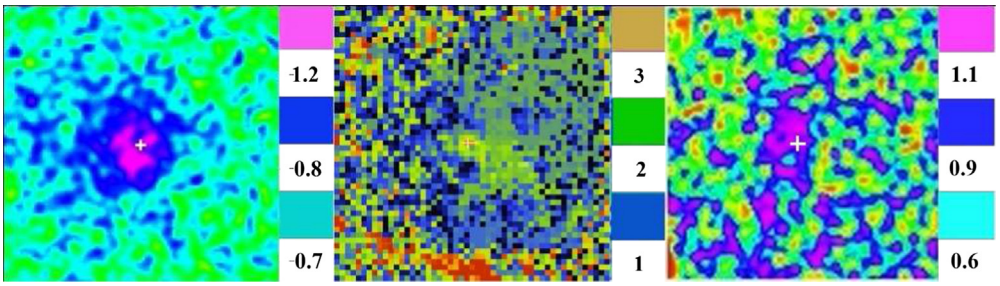

Fig. 3. Polarization map, from left: October 2011; January 2012; February 2012 respectively at phase angles of 15.2°, 28.3°, 25.5°. Polarization values are in %. The field of views, the North, the East and the solar directions are same as in Fig. 2.

A solar–antisolar asymmetry is confirmed from the contours of the intensity images. From the intensity images treated by the rotation gradient method, an ejection of materials along the antisolar direction is apparent in the case of January and February, 2012 observations at a phase angle of 28.3° and 25.5° respectively. But there is no indication of such distinct structure in October 2011 images. Only a small structure can be noticed. Among the three sets of observations, the least distance (1.21 au) of the comet from earth was in October. But at that time, comet's distance from sun was largest (2.12 au) and the phase angle was lowest (15.2°). At such small phase angle the ejected materials along the solar–antisolar direction are almost in the line of sight of the observer. This fact, together with the largest solar distance of the comet might have caused an apparent suppression of structures along the solar–antisolar direction during October 2011.

4.2. Polarization phase curve

Polarization values as a function of phase angle are characteristic of average physical properties of cometary dust. In Fig. 4, the polarization values reported in Table 3 are plotted as a function of phase angle and are compared to the polarimetric phase curves of the so-called 'high-P_{max} comets' and 'low-P_{max} comets' [18,5]. The synthetic polarization phase curves are fitted by trigonometric fits for the two classes and the wavelength domains. From Table 3, data with sufficiently large apertures are chosen for plotting to cover the polarization of whole coma.

Three classes of comets have been defined based on the maximum polarization value and more generally the positive branch on the polarimetric phase curve. These are: (1) 'low-P_{max} comets': with a low maximum polarization of about (18 ± 3)%, (2) 'high-P_{max} comets': with a higher maximum polarization of about (27 ± 3)%, and (3) 'Hale–Bopp comets': with a positive polarization higher than all other comets (although only observed up to $\alpha=48°$) [17,5,6]. The origin of this is not yet completely explained. For example, Kolokolova and Kimura [15] had suggested slowly moving large and compact particles for low-P_{max} comets and submicron-sized grains in fluffy aggregates for high-P_{max} comets. Such different kinds of particles are sometimes found in the same comet at different orbital epochs [9]. It is noted that the phase angle and slope at inversion seem to be slightly higher for high-P_{max} comets than the low-P_{max} ones [17].

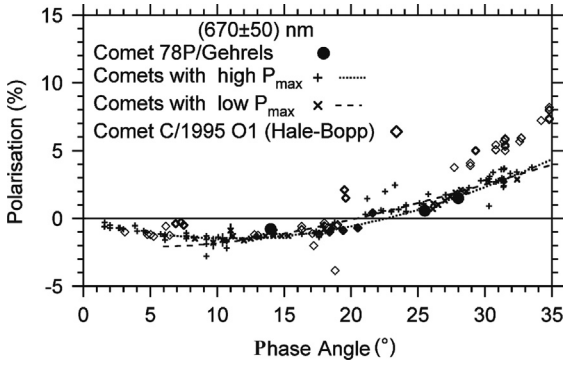

Fig. 4. Comparison of comet 78P/Gehrels whole coma polarization values to other comets polarization.

At low phase angles (lower than 35°), the synthetic phase curves are very close to one another. In the case of Gehrels, it is difficult to conclude from the present observations. It is just sure that Gehrels is not similar to comet Hale–Bopp with numerous submicron-sized grains.

4.3. Polarization maps

The jet-like structures, observed in high-P_{max} comets, have usually a higher polarization than the surrounding coma and are well collimated. In low-P_{max} comets some high polarization regions may exist but their extension is often limited to regions close to the nucleus. In the case of Gehrels, on the polarization map of all the periods, no significant difference in polarization values is noticed along the tailward structures and the surrounding coma. The only higher polarization region is observed just after perihelion in the solar direction in January. There are some past observations where enhanced gradient region did not present any polarimetric difference with the surroundings. For example, at $\alpha=18°$, the tailward structure (on the intensity image) of comet 22P/Kopff had the same polarization as the background [6]. At $\alpha=6.9°$, for comet C/1995 O1 (Hale–Bopp), the large structure perpendicular to the solar direction has the same polarization as the background, out of five jets detected around the photometric center [6]. The absence of difference in polarization suggests similar properties of the particles along the structures and the surrounding coma.

4.4. Comparative study with other results

Through the post-perihelion observations in 2004, Mazotta Epifani and Palumbo [20], observed similar coma shape with an important solar–antisolar asymmetry. The slopes of decrease in intensity are deeper at this period but the conclusions are similar with an important effect of solar radiation pressure and a well-defined tailward feature in the treated intensity images. The ejection in the solar direction seems to be more important and more extended in January, 2012. The higher polarization in the jets indicates that freshly ejected particles are slightly different from background particles. For those pushed in the tailward direction, the higher polarization is no more observed. Some of the particles can lose some carbonaceous compounds or be fragmented, but the snapshot observations do not allow us to interpret the difference further.

According to Mazotta Epifani and Palumbo [20], and their $Af\rho$ determination, comet Gehrels is a very dusty comet. $Af\rho$ is a proxy of dust activity with 'A' the grain albedo, 'f' the filling factor in the aperture and 'ρ' the linear aperture in cm [1]. This is compatible with the absence of emission lines [4]. The absence of well-focused jets suggests a low-P_{max} comet but this classification is not straightforward for phase angles smaller than 35°. It is interesting to note that a dusty comet is generally considered as a high-P_{max} [3,15].

The red color of the dust, found by Mazotta Epifani and Palumbo [20], is in favor of large particles in the coma and particles made of, or covered by carbonaceous compounds as suggested by experiments on analogs [7,8]. The polarization measurements suggest that jets with submicron-sized aggregates, such as found in well-focused jets of high-P_{max} comets or Hale–Bopp, are not ejected at the time of these observations. Nevertheless, the particles being very sensitive to the solar radiation seem to be porous.

5. Conclusion

Comet 78P/Gehrels 2 was observed from India and France during three periods from October 2011 to February 2012. They are (i) from IGO, India, in October 2011; about 3 months before perihelion, at a phase angle of 15.2°, (ii) from OHP, France, in January 2012; about 12 days after perihelion, at a phase angle of 28.3°, (iii) from IGO, India, in February 2012; about 1 month after perihelion, at a phase angle of 25.5°. From the polarization phase curve, it is evident that the positive branch of comet 78P/Gehrels is below that of the very active comet Hale–Bopp, but at such low phase angles it is difficult to conclude between low-$P_{\max}$ and high-$P_{\max}$ class of comets to which it belongs. From the polarization map it is confirmed that, after perihelion, in January and February, the observed intensity structures along the tailward direction have similar properties to the background coma. The particles ejected in the solar direction in January seem to be relatively large and with a low number density, but this structure was no more observable in February. The nonexistence of important jet activity suggests a possibility for 78P/Gehrels to be a member of the low-P_{max} class of comets.

Acknowledgments

The author S.R.C. acknowledges ELS XIV organizers with heartfelt gratitude for the interesting conference and their help with funding. We gratefully acknowledge OHP and IUCAA for allocation of observation time. The authors thankfully acknowledge the Indo French Centre for the Promotion of Advanced Research (CEFIPRA), for their kind funding of project Grant no. 4507-1. Finally, we are very much thankful to anonymous reviewers of this paper for their useful comments, which we believe had improved the quality of this paper.

References

[1] A'Hearn MF, Schleicher DG, Feldman PD, Millis RL, Thompson DT. Comet Bowell 1980b. Astron J 1984;89:579–91.
[2] A'Hearn MF, Millis RL, Schleicher DG, Osip DJ, Birch PV. The ensemble properties of comets: results from narrowband photometry of 85 comets, 1976–1992. Icarus 1995;118:223–70.
[3] Chernova GP, Kiselev NN, Jockers K. Polarimetric characteristics of dust particles as observed in 13 comets. Comparisons with asteroids. Icarus 1993;103:144–58.
[4] Fink U, Hicks MD. A survey of 39 comets using CCD spectroscopy. Astrophys J 1996;459:729–43.
[5] Hadamcik E, Levasseur-Regourd AC. Dust evolution of comet C/1995 O1 (Hale–Bopp) by imaging polarimetric observations. Astron Astrophys 2003a;403:757–68.
[6] Hadamcik E, Levasseur-Regourd AC. Imaging polarimetry of cometary dust: different comets and phase angles. J Quant Spectrosc Radiat Transf 2003b;79–80:661–79.
[7] Hadamcik E, Levasseur-Regourd AC, Leroi V, Bardin D. Imaging polarimetry of the dust coma of Comet Tempel 1 before and after Deep Impact at Haute-Provence Observatory. Icarus 2007a;190:459–68.
[8] Hadamcik E, Renard J-B, Rietmeijer FJM, Levasseur-Regourd AC, Hill HGM, Karner JM, et al. Light scattering by fluffy Mg–Fe–SiO and C mixtures as cometary analogs (PROGRA2 experiment). Icarus 2007b;190:660–71.
[9] Hadamcik E, Sen AK, Levasseur-Regourd AC, Gupta R, Lasue J. Polarimetric observations of comet 67P/Churyumov–Gerasimenko during its 2008–2009 apparition. Astron Astrophys 2010;517:A86.
[10] Hadamcik E, Sen AK, Levasseur-Regourd AC, Gupta R, Lasue J, Botet R. Dust in Comet 103P/Hartley 2 coma during EPOXI mission. Icarus 2013;222:774–85.
[11] Hadamcik E, Sen AK, Levasseur-Regourd AC, Roy Choudhury S, Lasue J, Gupta R, et al. Dust coma of comet C/2009 P1 (Garradd) by imaging polarimetry. Meteorit Planet Sci 2014;49(1):36–44.
[12] ⟨http://ssd.jpl.nasa.gov/horizons.cgi⟩.
[13] ⟨http://sites.google.com/site/robsastropics/comets-78p-gehels⟩.
[14] ⟨http://cometography.com/pcomets/078p.html⟩.
[15] Kolokolova L, Kimura H. Effect of electromagnetic interactions in the polarization of light scattered by cometary and other types of cosmic dust. Astron Astrophys 2010;513:A40.
[16] Larson SM, Sekanina Z. Coma morphology and dust-emission pattern of periodic comet Halley. I. Higher-resolution images taken at Mount Wilson in 1910. Astron J 1984;89(4).
[17] Levasseur-Regourd AC, Hadamcik E, Renard JB. Evidence for two classes of comets from their polarimetric properties at large phase angle. Astron Astrophys 1996;313:327–33.
[18] Levasseur-Regourd AC. Polarization of light scattered by cometary dust particles: observations and tentative interpretations. Space Sci Rev 1999;90:163–8.
[19] Lowry SC, Weissman PR. CCD observations of distant comets from Palomar and Steward Observatories. Icarus 2003;164:492–503.
[20] Mazzotta Epifani E, Palumbo P. The dust coma environment of the short period comets 32P/Comas Sola, 56P/Slaughter-Burnham, and 78P/Gehrels2 from ground-based observations. Astron Astrophys 2011;525:A62.
[21] Ramaprakash AN, Gupta R, Sen AK, Tandon SN. An Imaging polarimeter for multiwavelength observations. Astron Astrophys Suppl Ser 1998;128:369–75.
[22] Renard J-B, Levasseur-Regourd AC, Dollfus A. Polarimetric CCD imaging of Comet Levy (1990). Ann Geophys 1992;10:288–92.
[23] Sen AK, Joshi UC, Deshpande MR, Prasad CD. Imaging polarimetry of comet P/Halley. Icarus 1990;86:248–56.
[24] Sen AK, Tandon SN. Two channel optical imaging polarimeter. In: Crawford DL, Craine ER, editors. Proceedings of SPIE on instrumentation in astronomy VIII, vol. 2198; 1994. p. 264–73.
[25] Snodgrass C, Lowry SC, Fitzsimmons A. Optical observations of 23 distant Jupiter family comets, including 36P/Whipple at multiple phase angles. Mon Not R Astron Soc 2008;385:737–56.

Planetary and Space Science 118 (2015) 193–198

Contents lists available at ScienceDirect

Planetary and Space Science

journal homepage: www.elsevier.com/locate/pss

Study of some comets through imaging polarimetry

S. Roy Choudhury [a,*], E. Hadamcik [b,c,d], A.K. Sen [a]

[a] Department Physics, Assam University, Silchar 788011, India
[b] Sorbonne Universités, UPMC Univ. Paris 06, LATMOS-IPSL, 11 Bld d'Alembert, 78280 Guyancourt, France
[c] CNRS/INSU, LATMOS-IPSL, LATMOS-IPSL, 11 bld d'Alembert, 78280 Guyancourt, France
[d] Université Versailles St-Quentin, LATMOS-IPSL, 11 bld d'Alembert, 78280 Guyancourt, France

ARTICLE INFO

Article history:
Received 27 January 2015
Received in revised form
21 April 2015
Accepted 15 June 2015
Available online 24 June 2015

Keywords:
Comets C/2007 N3 (Lulin)
C/2011 L4 (PANSTARRS)
290P/Jager
Scattering
Polarization
Cometary dust
Technique: imaging polarimetry

ABSTRACT

Comets C/2007 N3 (Lulin), C/2011 L4 (PANSTARRS) and 290P/Jager were observed at phase angles <40°; between 2009 and 2014; with the 0.8 m Telescope at Haute-Provence Observatory (OHP) in France. The observations were polarimetric and mainly carried out in the red and near infra-red wavelength domains to reduce gaseous contaminations. The overall shape of the coma of comet Lulin is about circular without evident jet structure. The coma of comet C/2011 L4 is enlarged in the antisolar direction. Jets in a fan-like structure have been noticed between position angles 135°–245° in the treated intensity images. A correlated higher polarization region is noted on the corresponding polarization map. The shape of the coma of 290P/Jager is slightly elongated in the antisolar direction. Deeper negative polarization is found in the inner coma. The whole coma polarization values of these three comets correspond to the synthetic phase curve for comets at similar phase angles and wavelength.

1. Introduction

Imaging polarimetry is a nice technique to investigate the optical and physical properties of dust grains ejected by comets when they approach the sun. Previous works by the polarimetric imaging method have revealed that different regions inside coma show some differences in polarization suggesting differences in physical properties of the dust particles. Jets, fan-like structures usually show a higher polarization than the background. In some comets, regions close to the nucleus are marked with a smaller positive value at phase-angles larger than the inversion angle and a deeper negative polarization at small phase angles. (e.g. Dollfus and Suchail, 1987; Sen et al., 1990; Hadamcik et al., 2003a,b, 2010, 2013, 2014). In the present work, three comets are studied. C/2007 N3 (Lulin), Comet C/2011 L4 (PANSTARRS), 290P/Jager were observed polarimetrically with the 0.8 m telescope of Haute-Provence Observatory (OHP) in France.

Comet C/2007 N3 (Lulin) was discovered by Ye Quanzhi and Lin Chi-Sheng on 11 July 2007 using the 41-cm (16 in) Ritchey-Chretien at Lulin Observatory, Nantou, Taiwan as a part of the Lulin Sky Survey project. Two months after its last perihelion (10 January 2009), the comet was observed during the period 17–20 March 2009 at a geocentric distance 0.9 au, while the phase angle varied between 35.7° and 36.7°.

Comet C/2011 L4 (PANSTARRS) was discovered by Richard Wainscoat (Institute for Astronomy, University of Hawaii) on 6 June 2011 with the 1.8-m "Pan-STARRS 1 Ritchey-Chretien telescope" at Haleakala, HI, USA. For our study, the comet was observed on 6 and 7 May 2013, two months after the perihelion (on 10 March 2013) at a geocentric distance 1.5 au and phase angle 38°.

Comet 290P/Jager (or 1998 U3 or 2013 N1) was discovered by Michael Jager with a 0.25-m, f/2.8 Schmidt camera. From OHP, it was observed on 27 & 28 January 2014 at a geocentric distance 1.3 au, when phase angle was 14°–15°.

2. Observations and data reductions

The observation log and data reduction procedure are discussed below.

2.1. Instruments

The observations were carried out with the 0.8 m Cassegrain telescope of the Observatory of Haute-Provence, "OHP" situated near Marseille, France (Observatory reference: 511).

Details on the instruments can be found in Hadamcik et al. (2010, 2013). In brief, the telescope has a focal ratio f/15; the field

* Corresponding author.
E-mail address: saumya.viv@gmail.com (S. Roy Choudhury).

http://dx.doi.org/10.1016/j.pss.2015.06.011
0032-0633/

of view for polarization imaging is 7 arcmin. The CCD camera has 2048×2048 pixels, back-illuminated, of 13.5 μm each. The resolution by pixel is thus 0.21 arcsec; the pixels are binned 4×4 giving a final resolution of 0.84 arcsec. There are four polarizing filters mounted on a rotating wheel. The direction of polarization axis of first one is called direction '00'. The polarization axes of the three others are oriented at 45° from one another. For each orientation, a polarized intensity image is recorded and they are called respectively I_{00}, I_{45}, I_{90}, I_{135}. To avoid tracking problems short exposures were used; as the comets were faint, the final polarized images were built by adding the 10–15 individual images for each position of the polarization axis. In this way signal-to-noise ratio is increased.

The intensity (I), the measured polarization (P), and polarization angle (θ) are calculated by the following expressions:

$$I = I_0 + I_{90} = I_{45} + I_{135} \quad (1)$$

$$P = 200\frac{\sqrt{(I_0 - I_{90})^2 + (I_{45} - I_{135})^2}}{I_0 + I_{90} + I_{45} + I_{135}} \quad (2)$$

$$\theta = 0.5 \arctan\left[\frac{I_{45} - I_{135}}{I_0 - I_{90}}\right] \quad (3)$$

2.2. Log of observations

The log of observations is presented below (Table 1), α=phase angle, PA=sun–comet radius vector position angle, Δ=distance of the comet from the earth, R=distance of the comet from the sun. The filters used are Thuan-Gunn red R_{OHP} 655 nm, $\Delta\lambda$ 90 nm and I_{OHP} 810 nm, $\Delta\lambda$ 150 nm.

2.3. Data reduction

Bias subtraction and flat field correction to all cometary images were applied. After that, centering of optocenter with a precision of 0.1 pixel was done with gravity center algorithm. The sky background was estimated from a region outside the coma and free of faint stars and was subtracted from each polarized image. For each set of four images, the stability of fluxes at different apertures of polarized components (I_0, I_{45}, I_{90}, I_{135}) is controlled by measuring fluxes of each individual polarized components at apertures of diameter 5, 10, 15 pixels. If a difference greater than 1% is detected between the fluxes ($I_0 + I_{90}$ and $I_{45} + I_{135}$) for 15 pixels on the successive images, the image is rejected because in less than ten minutes interval between the successive images, they have to be same. As mentioned in Section 2.1, the final polarized images are built by adding the 10–15 individual images for each position of the polarization axis and thus intensity I, Eq. (1) is calculated for the whole series.

3. Results

Azimuthally integrated radial profiles of intensity and profiles of decrease in intensity along solar and anti-solar directions are presented first in this section. Coma morphologies (obtained from intensity images) followed by aperture linear polarization and polarization maps are presented subsequently. The variation in polarization values is studied with increase in aperture and the polarization maps are obtained to detect variation in polarization in different regions inside the coma and declare any decisive relation with different structures.

3.1. Intensity images

Intensity images are obtained by adding two mutually orthogonal polarized components. The components are either (I_0, I_{90}) or (I_{45}, I_{135}). The successive intensity images thus obtained for a particular set are further added (I_0, I_{90}) or (I_{45}, I_{135}) to build the final intensity images.

3.1.1. Intensity radial profile

Decrease in intensity as a function of optocentric distance is measured for all the comets from the intensity images. It is done by calculating the intensity in one pixel thickness annulus and then dividing by the number of pixels in that annulus. The log of the intensity values as a function of log of radial distance (in km) from optocenter is called azimuthally averaged radial intensity log–log profile (Fig. 1).

For Lulin, the slope of decrease on the radial profile is found to be about −1 for radial distance larger than 1080 km from the optocentre. It is around −1.16 between 540 and 1080 km and −0.9 within the radial distance 540 km. The slope along anti-solar direction is −1.06 between 1080 and 1750 km and that between 400 and 1080 km is about −1.2. Along solar direction, the slope is −1.2 between 540 and 1080 km and −1 after 1080 km.

In case of C/2011 L4, for optocentric distance larger than 4700 km, the slope of radial profile is around −1.17. From 1170 to 4700 km, the slope is about −1.19; between 700 and 1170 km it is about −0.81 and within 700 km, it is about −0.6. Along solar direction, the slope is −1.05 between 700 and 1170 km and −0.98 between 1170 and 5870 km. Along anti-solar direction, it is −0.94 from 940 km to 1880 km; and −1.04 from 3050 km to 5870 km.

For Jager, the slope is around −1(−0.98) for optocentric distance larger than 1560 km. In a region from 780 km to 1560 km, it is about −1.09 and before 780 km, the slope is nearly −0.88. Along the solar direction, the slope changes from −1.64 between 780 and 1560 km to −1.02 between 1560 and 2530 km. That along anti-solar direction is −0.83 between 580 and 970 km and −1.03 between 970 and 1560 km.

Table 1
Log of observations.

The comet	Date of observation	α°	PA°	Δ (au)	R (au)	Resolution (km/pixel)	Filter, exposure time (sec) × number of images used
C/2007 N3 (Lulin)	17.03.2009						R_{OHP},20 × 15;I_{OHP},20 × 15
	18.03.2009	35.7	97	0.9	1.5	135	R_{OHP},10 × 18;I_{OHP},20 × 12
	19.03.2009	−36.7	−96				R_{OHP},10 × 20
	20.03.2009						R_{OHP},20 × 12
C/2011 L4 (PANSTARRS)	06.05.2013	38	310	1.5	1.3	235	R_{OHP},30 × 15
	07.05.2013		−309				R_{OHP},30 × 15;I_{OHP},30 × 12
290P/Jager	27.01.2014	14–15	104	1.3	2.1	195	R_{OHP},120 × 5
	28.01.2014		−103				I_{OHP},120 × 4

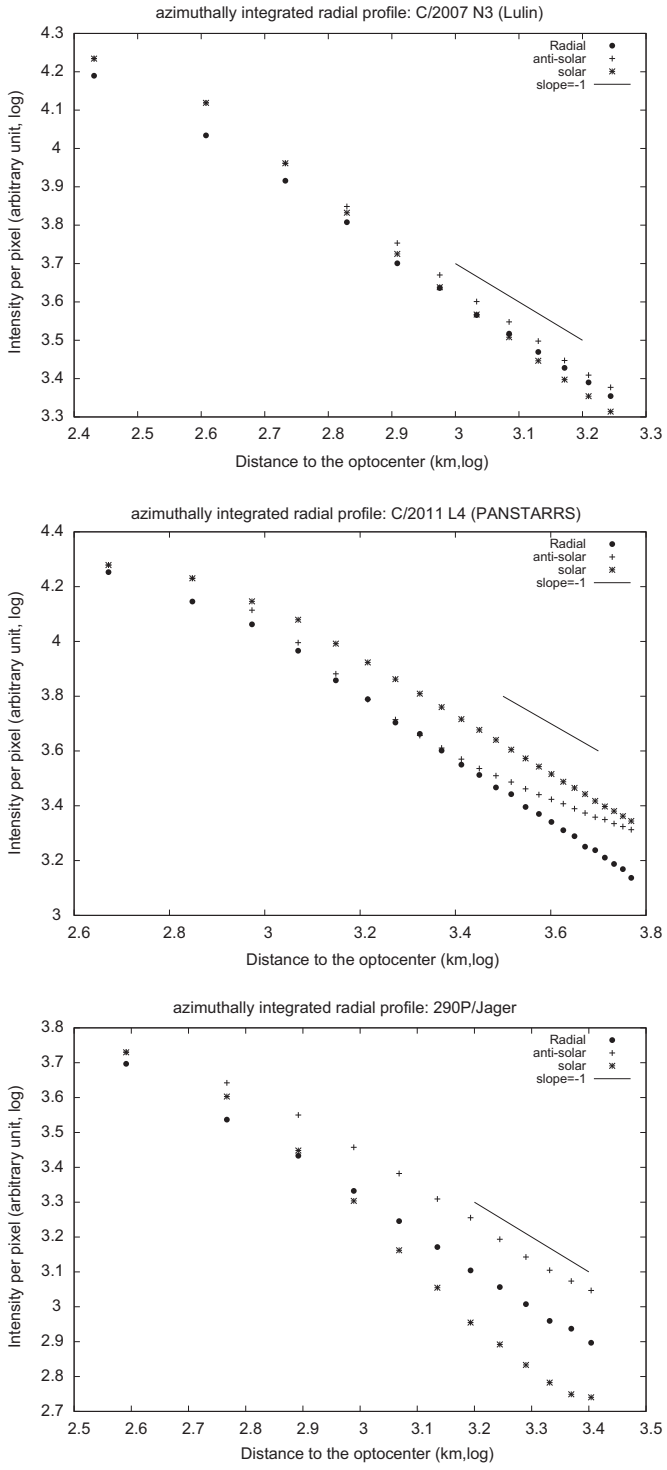

Fig. 1. Azimuthally integrated radial profiles of intensity and profiles of decrease in intensity along solar and anti-solar directions, as a function of optocentric distance in log–log scale for the three periods of observations and fits with −1 slope.

3.1.2. Coma morphologies

Isophotes and treated intensity images are presented (Fig. 2) in this section.

Isophotes: The isophotes reveal the shape of the coma in projection on the sky and suggest the presence and position angles of jets. They are here plotted in log scale for intensity.

Lulin was observed at phase angle 35.7°–36.7° with solar position angle 277°. The overall shape of coma is about circular with a slight elongation at about PA 190°, which can be consistent with a projected jet perpendicular to the solar direction. The coma of comet C/2011 L4 observed at a phase angle of 38°, is elongated in the antisolar direction; the solar position angle being 130°. In case of comet Jager, the coma has a slight extension in the anti-solar direction where during observation the solar position angle was 284° and phase angle 14°.

Treated intensity images: Intensity images were treated with the rotational gradient method introduced by Larson and Sekanina (1984). This emphasizes azimuthal intensity gradients, which help to identify structures if present.

No prominent structure has been noticed in case of Lulin. A fan-like structure has been noticed between position angles 135°–245° in the treated intensity images of C/2011 L4 corresponding to the enlarged shape of the isophotes in the South direction. Also, three jets on the South direction and two shorter jets in the North direction are noticed. In case of Jager, some small structures along the antisolar direction have been detected, which have a correlation to the elongated structures noticed on the isophotes. At low phase angle like 14°, materials ejected along the solar-antisolar direction are almost in the line of sight of the observer.

3.2. Linear polarization

The variation in polarization values with increase in aperture size is studied first. Finally, the polarization maps are obtained to detect variation in polarization in different regions of coma.

3.2.1. Aperture polarization

Integrated flux at a definite aperture is measured for each polarized component corresponding to four different positions of polarizer. For all the apertures, the fluxes are measured and the polarization is calculated using Eq. (2). The final polarization are presented in Table 2.

As often, a decrease in polarization values with increasing aperture is observed with an about constant value at larger apertures called whole coma polarization. Considering the error bars, the whole coma polarization values are nearly similar for the two filters- R_{OHP} and I_{OHP} and for the different nights, except in the inner coma where variations are currently observed.

3.2.2. Polarization maps

The polarization map of the three comets is shown in Fig. 3 in red wavelength. For Lulin, higher polarization is noticed surrounding the central coma, which decreases gradually. In case of C/2011 L4, a correlated higher polarization along the observed structures (on the rotational gradient image) is noticed on the polarization map. A deep negative polarization around central coma of Jager has been observed on its polarization map. Also, the polarization value decreases progressively with optocentric distance.

4. Discussion

4.1. Intensity variations in the coma

For Lulin and Jager, the slope of decrease of radial profile is about −1 (−1 for Lulin, −0.98 for Jager) at large optocentric distances. The −1 slope indicates an isotropic coma if the sky background is subtracted properly. For solar and anti-solar profiles, a slope greater than −1 (in magnitude) indicates that dust is moving away from the region; and that smaller than −1 (in magnitude) indicates that dust is replenishing the region. The slopes of Jager along solar and anti-solar direction clearly indicate that the dusts are pushed tailwards. For C/2011 L4, the slope is about −1 (solar −1.05, −0.97; anti-solar −1.04, −0.94) along solar

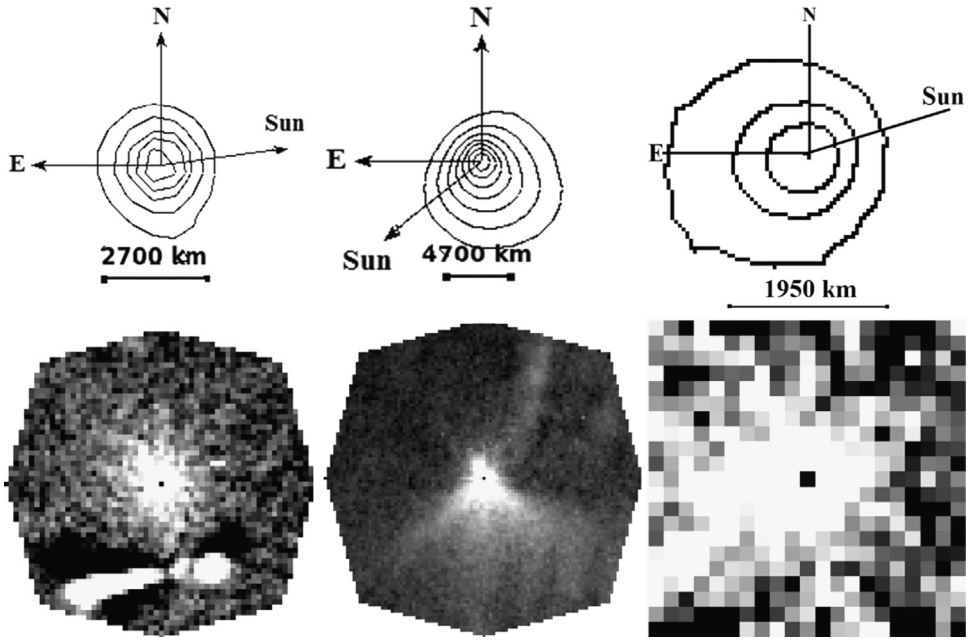

Fig. 2. Morphologies in intensity. From left - Lulin (17.03.2009), C/2011 L4 (07.05.2013), Jager (27.01.2014) in R_{OHP} at phase angles 35.7°, 38°, and 14° respectively. *Upper line*: isophotes are log scale for intensity. *Lower line*: images treated by rotational gradient method.

and anti-solar direction. And its radial slope (−1.18) is slightly higher (in magnitude) than −1 at outer coma; meaning that the dusts are not isotropically distributed on average. This is an indication for the presence of jets.

4.2. Polarization phase curve

In Fig. 4, the polarization values for the whole coma of the three comets (in red filter) have been plotted as a function of phase angle.

Classification of comets into different classes based on the synthetic phase curves (Levasseur-Regourd et al., 1996; Hadamcik and Levasseur-Regourd, 2003a) is generally possible if the polarization data are available for large phase angles (>35°). To fit all the data of comets to the three classes of comets, an empiric trigonometric function proposed by Lumme and Muinonen (1993) has been used-

$$P = b[\sin\ \alpha]^{c1}[\cos(\alpha/2)]^{c2}\ \sin(\alpha - \alpha_0) \quad (4)$$

Considering the error limits, the whole coma polarization values of Lulin, observed between 35° and 36° phase angle, seem to lie close to low-P_{max} class of comets. Woodward et al. (2011) observed the comet below 22°; their data are also plotted on the graph. Though at that phase angle the synthetic phase curves are very close to one another, yet it appears closer to low-P_{max} class within the error limits. Polarization values of C/2011 L4, observed at 39° phase angle seems to be closer to high-P_{max} class of comets. Jager was observed below inversion angle and as expected, low negative whole coma polarization is found.

4.3. Polarization maps

Higher polarization noticed surrounding the central coma of Lulin decreases gradually with radial distance from nucleus. In most of the cases, low-P_{max} comets show some high polarizations, limited to regions close to the nucleus (Kiselev et al., 2005; Hadamcik et al., 2007). In high-P_{max} comets, jet activity is more important and the jets extend far from the nucleus (Hadamcik and Levasseur-Regourd, 2003a; Hadamcik et al., 2014). The structures

Table 2
Polarization values P (in %) for different apertures and wavelengths.

Comet	Date	Filter	1080 (km)	2160 (km)	2980 (km)	4060 (km)	5140 (km)	5410 (km)
C/2007 N3 (Lulin)	17.03.2009	R_{OHP}	5.1 ± 0.3	4.9 ± 0.2	4.7 ± 0.2	4.3 ± 0.2	3.9 ± 0.2	3.9 ± 0.3
		I_{OHP}	3.3 ± 0.2	4.5 ± 0.2	4.5 ± 0.2	4.3 ± 0.2	4.0 ± 0.3	3.9 ± 0.3
	18.03.2009	R_{OHP}	3.9 ± 0.2	4.3 ± 0.2	4.3 ± 0.2	4.2 ± 0.2	3.9 ± 0.2	3.8 ± 0.3
		I_{OHP}	4.4 ± 0.2	4.3 ± 0.2	4.3 ± 0.2	3.9 ± 0.2	4.0 ± 0.3	4.0 ± 0.3
	19.03.2009	R_{OHP}	5.4 ± 0.3	5.1 ± 0.2	4.9 ± 0.2	4.5 ± 0.2	3.9 ± 0.3	3.9 ± 0.3
	20.03.2009	R_{OHP}	5.7 ± 0.4	5.2 ± 0.2	4.7 ± 0.2	4.4 ± 0.2	4.1 ± 0.2	4.0 ± 0.3
			2350 (km)	4230 (km)	6110 (km)	7990 (km)	9870 (km)	11750 (km)
C/2011 L4 (PANSTARRS)	06.05.2013	R_{OHP}	5.9 ± 0.3	5.9 ± 0.3	5.8 ± 0.3	5.7 ± 0.3	5.6 ± 0.4	5.5 ± 0.4
	07.05.2013	R_{OHP}	6.5 ± 0.4	6.1 ± 0.3	5.9 ± 0.3	5.8 ± 0.3	5.6 ± 0.4	5.5 ± 0.4
		I_{OHP}	6 ± 0.3	5.4 ± 0.3	5.2 ± 0.4	5.1 ± 0.4	star	star
			780 (km)	1170 (km)	1560 (km)	2340 (km)	3120 (km)	3900 (km)
290P/Jager	27.01.2014	R_{OHP}	−7.3 ± 0.5	−6.8 ± 0.3	−5.4 ± 0.2	−3.6 ± 0.2	−2.4 ± 0.2	−1.6 ± 0.2
	28.01.2014	I_{OHP}	−6.2 ± 0.4	−5.4 ± 0.2	−5.0 ± 0.2	−2.9 ± 0.2	−1.9 ± 0.2	−1.7 ± 0.2

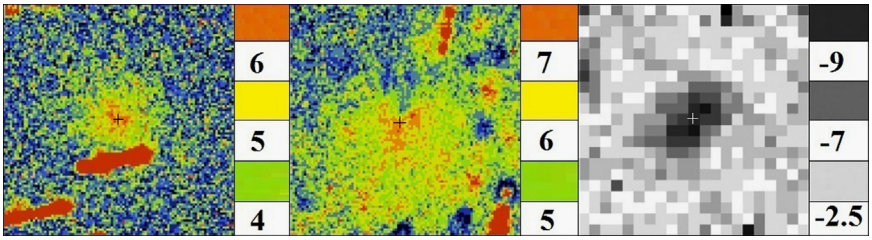

Fig. 3. Polarization map. From left – Lulin (17.03.2009), C/2011 L4 (07.05.2013), Jager (27.01.2014) in R_{OHP} at phase angles 35.7°, 38°,14° respectively. Polarization values are in %. Field of view for Lulin 13,700 × 13,700 km^2, for C/2011 L4 24,000 × 24,000 km^2, for Jager 4100 × 4100 km^2. N, E and solar directions are the same as in Fig. 2.

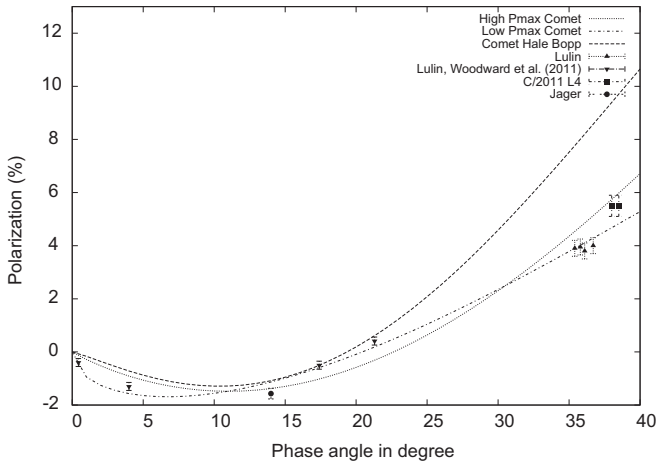

Fig. 4. Comparison of the polarization values obtained for the 3 comets in the present paper and the values obtained by Woodward et al. (2011) with the synthetic phase curves. Fitting all the data in the literature in the red wavelength domain for the 3 classes of comets.

noticed in case of C/2011 L4 have a higher polarization than the surrounding coma and are correlated to jets, confirming the classification of the comet among the high-P_{max} class. In some comets with an important seasonal effect such as comet 67P, jets can be observed in low-P_{max} comets (e.g. 67P) depending of the epoch of observations (Hadamcik et al., 2010). The deep negative polarization around central coma of Jager is called polarimetric halo. Such central polarimetric halo was observed in different comets (Hadamcik and Levasseur-Regourd, 2003b). Different compositions were suggested for this region but it is not yet resolved. The polarization is less negative in when the distance to the center increases. Higher polarization is detected along the observed jets. Comets belonging to the low-P_{max} class sometimes present less activity than high ones. E.g. CCD images of comet C/1989 X1 (Austin) do not present any jet structure (Eaton et al., 1992). Some other low-P_{max} comets present a high polarization near the nucleus and an important decrease of polarization as a function of aperture out of this region, e.g. 23P/Brorsen–Metcalf (Chernova and Kiselev, 1993) or 2P/Encke (Jockers et al., 2005). Nevertheless for this last comet, a lower polarization in the inner coma was found by Jewitt (2004) for some other period; this inner coma difference is discussed in Hadamcik and Levasseur-Regourd (2009). Kolokolova and Kimura (2010) suggested slowly moving large and compact particles for low-P_{max} comets and submicron-sized grains in fluffy aggregates for high-P_{max} comets.

5. Conclusion

With the 0.8 m telescope at Haute-Provence Observatory (OHP), France, some comets were observed between 2009 and 2014. Theses are (i) C/2007 N3 (Lulin), observed during 17–20 March 2009; at a phase angle between 35.7° and 36.7°, (ii) C/2011 L4 (PANSTARRS), observed on 6 and 7 May 2013; at a phase angle 38–39°, (iii) 290P/Jager, observed on 27 and 28 January 2014; at a phase angle 14–15°. The phase curve indicates the possibility of Lulin to be a low-P_{max} type of comet. In case of C/2011 L4, some jet structures, along north and south having a polarization higher than the surrounding coma have been noticed. This, along with phase curve confirms C/2011 L4 to be a high-P_{max} type of comet. Like 81P/Wild2, 22P/Kopff; the deep negative polarization around central coma called polarimetric halo is noticed in case of 290P/Jager. A small jet is also detected along anti-solar direction.

Acknowledgments

We thank D. Bardin for his help during the observations and acknowledge OHP for allocation of observation time. We also acknowledge the Program National of Planetology (PNP) and the Indo French Centre for the Promotion of Advanced Research (CEFIPRA project grant no. 4507-1) for their kind funding for observation. The author S. Roy Choudhury thankfully acknowledges Federation of Finnish Learned Societies and CEFIPRA for providing financial support to attend ACM 2014.

References

Chernova, G.P., Kiselev, N.N., Jockers, K., 1993. Polarimetric characteristics of dust particles as observed in 13 comets: comparisons with asteroids. ICARUS 103:1, 144–158.
Dollfus, A., Suchail, J.L., 1987. Polarimetry of grains in the coma of P/Halley I. Observations. Astron. Astrophys. 187, 669–688.
Eaton, N., Scarrott, S.M., Gledhill, T.M., 1992. Polarization studies of comet Austin. MNRAS 258, 384–386.
Hadamcik, E., Levasseur-Regourd, A.C., 2003a. Dust evolution of comet C/1995 O1 (Hale–Bopp) by imaging polarimetric observations. Astron. Astrophys. 403, 757–768.
Hadamcik, E., Levasseur-Regourd, A.C., 2003b. Imaging polarimetry of cometary dust: different comets and phase angles. J. Quant. Spec. Radiat. Transf. 79–80, 661–679.
Hadamcik, E., Levasseur-Regourd, A.C., Leroi, V., Bardin, D., 2007. Imaging polarimetry of the dust coma of Comet Tempel 1 before and after Deep Impact at Haute-Provence Observatory. Icarus 190, 459–468.
Hadamcik, E., Levasseur-Regourd, A.C., 2009. Optical properties of dust from Jupiter family comets. Planet. Space Sci. 57:10, 1118–1132.
Hadamcik, E., Sen, A.K., Levasseur-Regourd, A.C., Gupta, R., Lasue, J., 2010. Polarimetric observations of comet 67P/Churyumov–Gerasimenko during its 2008–2009 apparition. Astron. Astrophys. 517, A86.
Hadamcik, E., Sen, A.K., Levasseur-Regourd, A.C., Gupta, R., Lasue, J., Botet, R., 2013. Dust in Comet 103P/Hartley 2 coma during EPOXI mission. Icarus 222, 774–785.
Hadamcik, E., Sen, A.K., Levasseur-Regourd, A.C., Roy Choudhury, S., Lasue, J., Gupta, R., Botet, R., 2014. Dust coma of comet C/2009 P1 (Garradd) by imaging polarimetry. Meteor. Planet. Sci. 49 (Nr 1), 36–44.
Jewitt, D., 2004. Looking through the hippo: nucleus and dust in comet 2P/Encke. Astronom. J. 128, 3061–3069.
Jockers, K., Kiselev, N., Bonev, T., Rosenbush, V., Shakhovskoy, N., Kolesnikov, S., Efimov, Yu., Shakhovskoy, D., Antonyuk, K., 2005. CCD imaging and aperture polarimetry of comet 2P/Encke: are there two polarimetric classes of comets?. Astron. Astrophys. 441, 773–782.

Kiselev, N.N., Rosenbush, V., Jockers, K., Velichko, S., Kikuchi, S., 2005. Database of comet polarimetry: analysis and some results. Earth Moon Planets 97 (3–4), 365–378.
Kolokolova, L., Kimura, H., 2010. Effect of electromagnetic interactions in the polarization of light scattered by cometary and other types of cosmic dust. Astron. Astrophys. 513, A40.
Larson, S.M., Sekanina, Z., 1984. Coma morphology and dust-emission pattern of periodic comet Halley. I. Higher-resolution images taken at Mount Wilson in 1910. Astronom. J. 89 (4).
Levasseur-Regourd, A.C., Hadamcik, E., Renard, J.B., 1996. Evidence for two classes of comets from their polarimetric properties at large phase angle. Astron. Astrophys. 313, 327–333.
Lumme, K., Muinonen, K., 1993. A two-parameter system for linear polarization of some solar system objects. In: IAY Symposium 160: Asteroids, Comets, Meteors, p. 194.
Sen, A.K., Joshi, U.C., Deshpande, M.R., Prasad, C.D., 1990. Imaging polarimetry of Comet P/Halley. Icarus 86, 248–256.
Woodward, C.E., Jones, T.J., Brown, B., Ryan, E.L., Krejny, M., Kolokolova, L., Kelley, M. S., Harker, D.E., Sitko, M.L., 2011. DUST IN COMET C/2007 N3 (LULIN). Astronom. J. 141:181 (9 pp).